

DIPLOMARBEIT

Constraining uncertainty in climate projections from the 8.2 ka event and its influence on a hedging strategy against global warming impacts

Alexander Lorenz

18. Oktober 2007



angefertigt am Potsdam-Institut für Klimafolgenforschung
eingereicht am Institut für Physik der Universität
Potsdam

Abstract

Although climate system models can reproduce a variety of real climate-related phenomena, the usefulness of these models for projections of future climate evolution is constrained by their reliability. Models have to be imperfect by construction because of limited resolution in spatiotemporal dimensions and in processes explicitly represented. Processes below this resolution are handled by parameterization including free tuning parameters. Thus the uncertainty of important climate parameters results in a folder of potential climate projections rather than one precise projection. Generically uncertainty of a projection will be reduced when requesting that model parameter settings must result in model output that is consistent with already observed data Bayesian Learning provides one well-defined procedure to weigh parameters accordingly in case prior uncertainty can be expressed by a probability measure.

This study presents a scheme how to Bayesian learn from paleoclimatic data, including in particular the 8.2 ka event, on CLIMBER-2.3 ocean parameters, to reduce their uncertainty. As the 8.2 ka event represents an outstanding climatic anomaly it is assumed to show high potential for the reduction of parameter uncertainty (contains much information). While previous Bayesian paleo-studies with CLIMBER-2 focused on reducing uncertainty in Climate Sensitivity, the 8.2 ka event can be expected to strongly correlate with so far uncertain ocean diffusivity properties. Only by utilizing a stochastic version of CLIMBER-2.3 Bauer et al. (2004) has been able to mimic the 8.2 ka event achieving a suitable long duration of cooling. Employing this version of CLIMBER-2.3 the technical difficulty arises to have to numerically establish the related likelihood in addition to the uncertain model parameters: While mainstream uncertainty analyses can assume a quasi-Gaussian shape of likelihood, with weather fluctuating around a long term mean, the 8.2 ka event as a highly nonlinear effect precludes such an a priori assumption. As a result of this study the Bayesian Learning showed a reduction of uncertainty in ocean diffusivity parameters of factor 3 compared to prior knowledge. This learning effect on the model parameters is transferred to other model outputs of interest like the inverse ocean heat capacity, which is important for the time scale of climate response to anthropogenic forcing. As an outlook, the economic implications of this development are discussed.

Contents

1	Introduction	1
1.1	The 8.2 ka event	2
1.2	Ensemble simulations for constraining model parameters	4
2	Theory & Methodology	5
2.1	Bayesian Learning	5
2.1.1	Application of Bayesian Learning	6
2.1.2	Constructing the likelihood	6
2.2	Model and data	8
2.2.1	The Greenland ice core data	8
2.2.2	CLIMBER-2.3	11
2.2.3	Methodology of model-data intercomparison	12
3	Simulation experiments	17
3.1	The 8.2 ka event in CLIMBER-2.3	17
3.1.1	Experimental setup	17
3.1.2	Sampling strategy	18
3.2	Summary	21
4	Results & Interpretation	23
4.1	Interpretation of the 8.2 ka event in CLIMBER-2.3	23
4.2	The histogram of cold event duration	24
4.3	Constructing the likelihood	29
4.3.1	Conditional likelihood of ocean diffusivity parameters a_{hoc} and a_v	30
4.4	Transforming the learning effect to relevant climate parameters	31
4.4.1	Transient Climate Response (TCR)	31
4.4.2	Climate Sensitivity ($T_{2\times\text{CO}_2}$)	33
4.4.3	Climate response parameter α_{res}	35
4.5	Summary	39
5	Discussion	41
5.1	Using additional sources of information - Autocorrelation of salinity- and temperature field data	42
5.2	Including additional parameters; strength FW of baseline flux	45
5.3	Impact of the learning effect on climate policy	46

Contents

6 Summary & Outlook	51
Zusammenfassung in deutscher Sprache	52
List of figures	57
References	58
List of abbreviations	64

1 Introduction

“Ours is an uncertain world” [Howson and Urbach (1991)]. This holds especially when considering complex systems like Earth’s climate. Whether the uncertainty arises from our own imperfections such as incomplete knowledge of causalities and limited computational ability or from internal fluctuations in the world itself - it challenges our knowledge of the future. So any attempt to predict the future evolution of Earth’s climate system rests on guessing the future based on today’s knowledge. Modeling the climate is a more sophisticated version of guessing as the climate models embody our knowledge in a self consistent and formalized way. In these models one part of our uncertainty is represented by free tuning parameters. Thus the results of modeling show a variety of possible future evolutions given a prescribed anthropogenic forcing. The central question remains unsolved: How to distinguish between good and bad ‘guesses’. One possible answer is to trust those models that can reproduce the system’s states in the past and then trusting only in those parameter settings when predicting the future.

While a validation of models by ‘assimilating’ data establishes trust into model structures by dividing parameter settings into ‘yes’ and ‘no’ on the base of a few data sets, the Bayesian Learning, formally be described by Bayes’ Theorem (see chapter 2.1), interpolates between ‘yes’ and ‘no’ for parameter settings in a probabilistic manner. Previous Bayesian paleo-studies with CLIMBER-2.3 focused on reducing uncertainty of Climate Sensitivity, i.e. *equilibrium properties* (for model description see section 2.2.2). The key idea of this thesis is to Bayesian learn from another pool of paleo-data, containing the prominent 8.2 ka event (see section 1.1), that can be expected to correlate with effective ocean heat capacity. The latter is of high interest as it strongly determines the *time scale* of climatic response to greenhouse gas forcing, hence (together with climate sensitivity) provides valuable input for climate policy. Previous work [Bauer et al. (2004)] has shown that CLIMBER-2.3 is able to mimic the 8.2 ka event. But only by using a stochastic version, including noisy freshwater forcing, the correct duration of cooling could be achieved. This thesis rests on the assumption that the event is strongly influenced by ocean diffusivities that in turn co-determine ocean heat capacity. So it aims at a Bayesian Learning influence chain from the 8.2 ka event onto the time scale of climate response in a dynamically consistent way, within the stylized world of CLIMBER-2.3.

In the following sections the current literature of the 8.2 ka event and the general approach of model-data comparison are summarized. The theoretical background of the method called Bayesian Learning is elaborated in chapter 2 followed by the

1 Introduction

methodological tools employed in this study. In chapters 3 and 4 the main task of this study, namely the application of Bayesian Learning to constrain uncertainty of model parameters, is carried out in detail. The resulting learning effect on model parameters is then transferred to other output like TCR, T_{2CO_2} and the inverse ocean heat capacity which is important for the time scale of climate response to anthropogenic forcing. The results are discussed in chapter 5 and first steps are taken to answer the arising questions. The conclusion is followed by implications for further research (see section 6).

1.1 The 8.2 ka event

The so called 8.2 ka event (or 8k event) refers to an outstanding cooling event in paleoclimate records at approximately 8200 years before present (BP before 1950, that is 8240 before 2000 [b2k]) [Rohling and Pälike (2005), Alley and Ágústsdóttir (2005), Thomas et al. (2007)]. The event was first reported in the Greenland ice core records as an abrupt cooling of about $6 \pm 2^\circ\text{C}$ at Summit, Greenland, which lasted roughly two centuries [Johnsen et al. (1992), Dansgaard (1993), Alley et al. (1997)]. Since then much has been published about the characteristics of this event, concerning the duration, the range, the driving mechanisms and the implications. Thomas et al. (2007) (where one can find a comprehensive overview over the discussion) describes the 8.2 ka event as a 160.5 yr cold period (from about 8250 – 8090 BP), where decadal mean isotopic values were below the early Holocene average (9.3-8.3 kyr BP). The minimum of $\delta^{18}\text{O}_{\text{ice}}$ ¹ is observed in the GRIP ice core at a calendar date of 8190 BP, dated on the GICC05 age scale [Rasmussen et al. (2006a)]. Under use of nitrogen isotopic data as a calibration tool Leuenberger et al. (1999) report a best estimate of 7.4 K for the magnitude of temperature change at Summit. Besides reduced Greenland temperature the northern climate during the 8.2 ka event was characterized by a fresher and colder North Atlantic Ocean, drier and stronger winds over the northern Atlantic, drier monsoon regions and intensified North Atlantic trade winds, according to Alley et al. (1997). A variety of additional paleoclimatic data from locations in the Northern Hemisphere (NH) show climate anomalies in the same time regime (overview of references from Bauer et al. (2004)). So e.g. Klitgaard-Kristensen et al. (1998), von Grafenstein et al. (1999) concluded that the cold event did not only have a regional but at least a hemispherical range. In a more recent paper Rohling and Pälike (2005) argued that the data found outside the North Atlantic region show only weaker signals of longer duration in this period and they concluded that the registered cooling has to be a superposition of a sharp and at least one other broad anomaly. That places doubts on the hemispherical

¹During the event $\delta^{18}\text{O}_{\text{ice}}$ drops about 1.5 ‰, which corresponds to a surface air temperature decrease of 3-6 K depending on the transformation method [e.g. Johnsen et al. (1995), Cuffey and Clow (1997), Johnsen et al. (2001)].

range of the event and emphasises the necessity of a detailed assessment of the event(s) around 8.2 kyr BP. To avoid this discussion in the present study the use of data representing the 8.2 ka event is constrained to the Greenland ice cores. The question of the cause of the 8.2 ka event has been addressed by different suggestions. Muscheler et al. (2004) investigated a change in solar forcing as a possible trigger for the cooling event by analysing ^{10}Be isotope data from the GRIP ice core and tree-ring $\delta^{14}\text{C}$ records. They concluded that the 8.2 ka event started in a phase of decreasing solar forcing, so the variable sun activity could only have been a trigger to start the event but that it is most probably not the main cause for this climate deterioration. By using model simulations Wiersma and Renssen (2006) have shown that the ocean is able to play an important role in amplifying centennial-scale climate variability such as variations in solar forcing. Considering this amplifying effect the solar forcing might be able to induce cooling phases in the Holocene (also see [Renssen et al. (2006)]).

As an alternative it is generally suggested that freshwater fluxes caused the cold event by having induced a weakening of deep water formation in the Northern Atlantic and therefore reduced northward heat transport by the Atlantic Thermohaline Circulation (THC) [Barber et al. (1999), Clark (2001), Rahmstorf (2002)]. Numerous model simulations have been performed [e.g. Renssen et al. (2001), Renssen et al. (2002), Bauer et al. (2004), Wiersma and Renssen (2006)] that have been able to reproduce an asymmetric cold event induced by freshwater pulses of different strength and duration. Evidence of the drainage of glacial lakes Agassiz and Ojibway in an outburst at about 8470 BP [Liccardi et al. (1999), Leverington et al. (2002), Teller et al. (2002)] deliver a plausible scenario of a strong pulse-like freshwater forcing to the North Atlantic region for the time of interest. Employing the CLIMBER-2 model Bauer et al. (2004) were able to reproduce a cold event with a duration that exceeded the scale of the freshwater forcing considerably by using a pulse-like drainage of 2.6 Sv, released for two years.

Ganopolski and Rahmstorf (2001) found in model studies that the sensitivity of the climate system to freshwater forcing not only depends on the properties of the forcing, such as its rate, its total volume and the forcing region, but also on the climate state itself. So the suggestions of possible causes were combined by Rohling and Pälike (2005) and Alley and Ágústsdóttir (2005) to explain the findings in the way, that solar forcing caused a cooling on longer scales of about 400-600 years. Within this colder period with possibly increased sensitivity to freshwater forcing the outburst from the pro glacial lakes then would have caused the prominent 8.2 ka event.

So Thomas et al. (2007) concluded, as the interest in the 8.2 ka event is currently high, with increasing numbers of paleoclimate data recording this period and with the event being used to test climate models' performance, that it is of enormous importance to gain a better understanding of the mechanisms behind this event.

1.2 Ensemble simulations for constraining model parameters

As the available computing ability is limited, any climate system model has to be incomplete in the sense that not all processes can be directly resolved and computed. The models account for this incompleteness by introducing parameterizations that involve tuning parameters to describe the left-out processes in an aggregated manner. Tuning of these parameters can lead to a very different model output, so choosing different values of tuning-parameters represents a whole ensemble of possible different climate models (or different realizations of one climate model). Regarding parameters as uncertain, generically introduces additional uncertainty.

When driven with the same forcing, these different climate model realizations will show different climate scenarios. If for a given period of time the forcing of the climate system and the corresponding climate characteristics (e.g. temperature, precipitation patterns,...) are known with high certainty, one has the possibility to rule out or at least discount some of the parameter settings. The different model realizations are all driven by the same forcing and the resulting output is compared to the measured climate characteristics and the parameter settings are discounted accordingly. This method possibly constrains the values of some of the unknown parameters in the climate model and therefore reduces the uncertainty about those parameters. As the possible future climate scenarios also depend on the (now constrained) model parameters, the range of possible future climate evolution may also decrease. In the same way, other important indicators of future climate evolution, like Climate Sensitivity ($\Delta T_{2\times CO_2}$), Transient Climate Response (TCR) or the distance to bifurcations in the climate system, are linked to model parameters and can be constrained by this method. This *learning step* can be described by Bayes' Formula.

When considering the comparison of models to paleo-data the reconstruction of past climate characteristics faces different difficulties (e.g. dating errors, transformation between different characteristics [$\delta^{18}O_{ice}$ to T]) as new sorts of uncertainties are involved.

Nevertheless to maximize the learning effect on the parameters under investigation it is advisable not only to compare model output to present day climate but also to different aspects of paleoclimate, as done by von Deimling et al. (2006). This is due to the fact that for present-day observations the signal to noise ratio 'temperature vs. CO₂ concentration' is rather low.

2 Theory & Methodology

2.1 Bayesian Learning

This study refers to the subjective Bayesian Theory as presented by Howson and Urbach (1991), as a theory of uncertainty. At the heart lies Bayes' Theorem:

$$P(h|e) = \frac{P(e|h)P(h)}{P(e)} . \quad (2.1)$$

It follows directly from the assumption of the four so called axioms of probability theory and the Dutch book theorem (see [Howson and Urbach (1991)]) and it delivers a calculus how the *subjective probability* of hypothesis h has to be altered facing the evidence e . Thereby $P(h)$ is the prior probability of hypothesis h , $P(e|h)$ is the likelihood of h on e , $P(h|e)$ is the posterior probability of h on e and $P(e)$ is the probability of e without “knowing” h . The probabilities are subjective because they merely reflect the personal degree of belief in h instead of claiming some objective property of hypothesis h . This is incorporated in the calculus by the need of a prior probability. Bayes' Theorem is additive in the sense that the formula can be iterated when additional data (or evidence) occurs. The former posterior probability is then used as the new prior for each additional Bayesian Learning step. It can be shown that finally the posterior probability is insensitive to the prior, in the sense that two people starting from very different prior beliefs must converge in their posterior beliefs as evidence accumulates. Hence the Bayesian approach delivers an objective tool for handling uncertainty that leads to an intersubjective consensus (but not to objective probability of h). In practical application of Bayes' Formula one might face difficulties. It is not clear how to use the probability $P(e)$ of the evidence without knowing h as the data are only considered in context of the hypothesis h . As a consequence of the probability axioms $P(e)$ can be rewritten as

$$P(e) = P(e|h)P(h) + P(e|\sim h)P(\sim h)$$

where $\sim h$ is the negation of h . Substituting in equation (2.1) one gets

$$P(h|e) = \frac{P(h)}{P(h) + \frac{P(e|\sim h)}{P(e|h)}P(\sim h)} . \quad (2.2)$$

This means that the posterior probability $P(h|e)$ only depends on the prior $P(h)$ and the so called likelihood ratio $P(e|\sim h)/P(e|h)$. If h' implies $\sim h$, that is if it

2 Theory & Methodology

is an alternative to h in explaining e it is easy to see that $P(e|h)$ increases with $P(e|h')P(h')$. But this implies that the degree of belief in h decreases with the extent of the explanatory power assigned to alternative hypotheses. This causes a serious problem as for each h there exist infinitely many alternative explanations h' with non-zero prior probability. Thus in practical usage one has to constrain the domain of hypotheses to a finite support.

2.1.1 Application of Bayesian Learning

In this study the model CLIMBER-2.3 is compared to observations from paleo-data containing the 8.2 ka event to reduce uncertainty of model parameters α (i.e. a vector). This learning effect is to be transferred to another output of interest (e.g. $z = \text{TCR}$ or $z = \Delta\mu$; see section 4.4), which is determined by $z = g(\alpha)$. The model parameters α are chosen to contain the horizontal and vertical ocean diffusivity (a_{hoc}, a_v), which are supposed to have strong influence on the model performance at reproducing the 8.2 ka event. The comparison is complicated by the fact that the 8.2 ka event in CLIMBER-2.3 not only depends on α but also on a particular realization η of noisy freshwater forcing. The methodology after which transformations “CLIMBER-2.3n” (the noisy version of CLIMBER-2.3) can be compared to observations is explicated in section 2.2.3. Bayes’ Formula then reads

$$P_{\text{post}}(\alpha) = \frac{P_{\text{prior}}(\alpha) P(y|\alpha)}{\int d\alpha' P_{\text{prior}}(\alpha') P(y|\alpha')} . \quad (2.3)$$

Thereby the hypothesis h is replaced by a certain realization of CLIMBER-2.3 that is characterized by a value of α of tuning parameters. As the choice of one value for α logically contradicts any other value the divisor becomes an integral over all values (a finite domain) of α and the probabilities become probability density functions on the same domain. The y denotes the observational spatiotemporal data in terms of CLIMBER-2.3 scale aggregated fields.

The transformation of the learning to model output z is then given formally by

$$P(z) = \int d\alpha P_{\text{post}}(\alpha) \delta(z - g(\alpha)) . \quad (2.4)$$

2.1.2 Constructing the likelihood

The central practical problem of this study is that when dealing with the 8.2 ka event for a given α the likelihood $P(y|\alpha)$ is not known a priori for CLIMBER-2.3n. If y were a scalar one could estimate $P(y|\alpha)$ by producing a suitable number (100...10000) of test runs with CLIMBER-2.3 (i.e. realizations of η). As this computational cost increases by a factor of $\approx 10^{n-1}$ if n is the dimension of y the information content of y is firstly reduced by nonlinear projection $y \rightarrow T$ on a quantity that preserves as much information as possible. This is chosen to be the

duration T of the cold event as it is highly sensitive towards the realization of η . The high-dimensional paleo-data y and model output y' are projected onto T by a Least Square Fit of a trapezoid function (see figure 2.2.1). As there is only one realization of T within nature (within the data) for any α , $P(T|\alpha)$ only needs to be reconstructed in the vicinity of that T .

In reality the data are obscured by weather noise not resolved in the CLIMBER-2.3 output of the 8.2 ka event. To ensure compatibility of model output and data weather noise of appropriate functional form is applied to the model's output. If the α domain is sampled by $\alpha_1, \dots, \alpha_i, \dots, \alpha_I$ per α a factorial sampling scheme¹ for η and ζ is set up. As only the realizations of the freshwater noise η enter CLIMBER-2.3n the addition of weather noise realizations ζ is computationally cheap. The likelihood is approximated by a histogram of bin-size ΔT , hence

$$\forall_i \in \{1, \dots, I\} \quad P_{\text{post}}(\alpha_i) \approx \frac{p_{\text{prior}}(\alpha_i) f_i}{\sum_i p_{\text{prior}}(\alpha_i) f_i} \quad (2.5)$$

where

$$f_i = \frac{1}{N_i} \sum_{jk} \text{Ind}(T_{ijk} \in [T - \Delta T/2, T + \Delta T/2]) \quad (2.6)$$

with j, k denoting the index of η and ζ , N_i the number of η and ζ realizations for each α_i . 'Ind' is the indicator function that is 1 if the boolean argument is true and 0 otherwise, $P(\alpha_i)$ denotes the finite probability for the realization α_i (the α domain is coarsely resolved), while p represents respective densities in analytic form.

For transforming the result to another output z the finite sample counterpart of equation (2.4) is used:

$$P(z \leq z^*) \approx \frac{\sum_i \text{Ind}(g(\alpha_i) \leq z^*) P_{\text{post}}(\alpha_i)}{\sum_i P_{\text{post}}(\alpha_i)}. \quad (2.7)$$

For the validity of this approach the convergence and the optimal choice of ΔT have to be ensured. Held (2007) proposes to bootstrap the following ensemble: The α_i whereby any α_i is found $m_i = \text{Ind}(T_{ijk} \in [T - \Delta T/2, T + \Delta T/2])$ times in the ensemble. From this ensemble the variance of z is plotted over ΔT and the minimum of the curve is identified. After fixing ΔT the sampling of CLIMBER-2.3n should be repeated to minimize multiple use of statistical information.

The optimal ΔT should fulfill an additional constraint: If the posterior variance of z is dominated by the likelihood (not by the prior; which is desirable) one is interested in the parameter α^* that maximizes the likelihood and the half-width of the likelihood in α along $\text{grad}(z)$. To be able to estimate this half-width

¹Each dimension of the parameter space is divided into equidistant intervals and samples are taken at every possible combination of values from all dimensions leading to a grid of sampling points in n-dimensional parameter space.

2 Theory & Methodology

reliably the relative counting error of the ratio of counts at the maximum K to counts at 1/2-level of likelihood $K/2$ should be small:

$$\delta \frac{K}{K/2} \approx \frac{1}{\sqrt{K}} + \frac{1}{\sqrt{K/2}} = (1 + \sqrt{2}) \frac{1}{\sqrt{K}} \ll 1. \quad (2.8)$$

with K either denoting the expected number of $\eta \otimes \zeta$ counts at α^* in case η, ζ have equal influence on the shape of $P(T|\alpha)$ or denoting the number of η counts in case η dominates $P(T|\alpha)$. In this study equation (2.8) rises a constraint focused more on the number $N_{j,k}$ of shots per α_i than on ΔT as the bin-size of the histogram is limited to $\Delta T = 20$ years by the resolution of the Greenland data.

2.2 Model and data

2.2.1 The Greenland ice core data

The data material representing the 8.2 ka event for the model-data intercomparison is chosen from the European Greenland ice core Project (GRIP) [GRIP-Project-Members (1993)], the parallel US Greenland ice sheet project 2 (GISP2) [Mayewski et al. (1994)] and the Dye 3 [Dansgaard (1985)] and North GRIP (NGRIP) ice cores [NGRIP-Project-Members (2004)]. Thomas et al. (2007) used

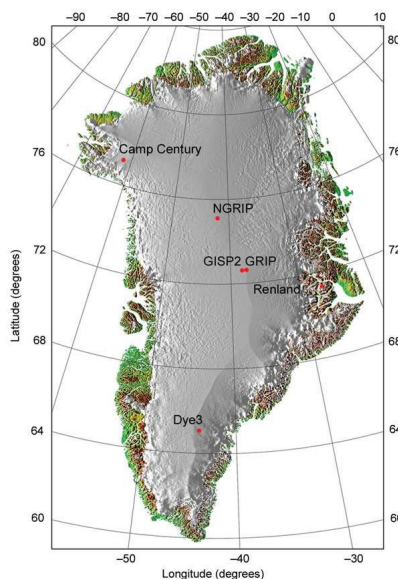


Figure 2.1: Locations of the deep ice core drilling sites: GRIP (72.5°N, 37.3°W), GISP2 (72.5°N, 38.3°W), NGRIP (75.1°N, 42.3°W) and Dye3 (65.2°N, 43.8°W) (the Greenland map by S.Ekholm, Danish Cadastre / published in Nature, 431, 147-151, 2004)

different isotope data to determine the duration and the structure of the 8.2 ka event. In this study only the $\delta^{18}\text{O}_{\text{ice}}$ data were taken into account synchronized to the GICC05 age scale with a resolution of 20 years as presented by Rasmussen et al. (2006b) (see figure 2.2.1). For the application of the Bayesian Learning the

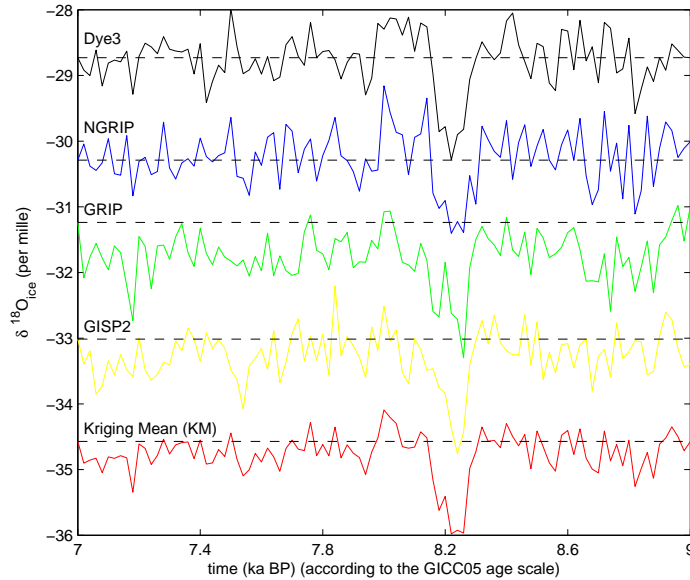


Figure 2.2: Time series of $\delta^{18}\text{O}_{\text{ice}}$ data from four Greenland ice cores and their Kriging Mean. Time series are offset by $+1.5\text{‰}$ each against the KM.

data are aggregated to CLIMBER-2 box scale according to the scheme in section 2.2.3. Naturally the next step would be the transformation of this Greenland-wide $\delta^{18}\text{O}_{\text{ice}}$ time series into a temperature record as the CLIMBER-2 output is in units of temperature. As there exists no general transformation function from $\delta^{18}\text{O}_{\text{ice}}$ to temperature, the absolute value of a so transformed record would be of no use for comparison to model output. So a different approach is used: Both the model output and the aggregated data are transformed to the duration of the event by a nonlinear fitting procedure of a trapezoid function (according to section 2.2.3), that takes into account the asymmetric evolution of the cold event. Thereby it is assumed that the duration T is roughly invariant under uncertainties of the $\delta^{18}\text{O}_{\text{ice}} \rightarrow T$ transformation. For the aggregated data this fitting is shown in figure 2.2.1. The resulting duration of the 8.2 ka event in the Greenland ice core data of 160 years is in good agreement with the findings of Thomas et al. (2007).

2 Theory & Methodology

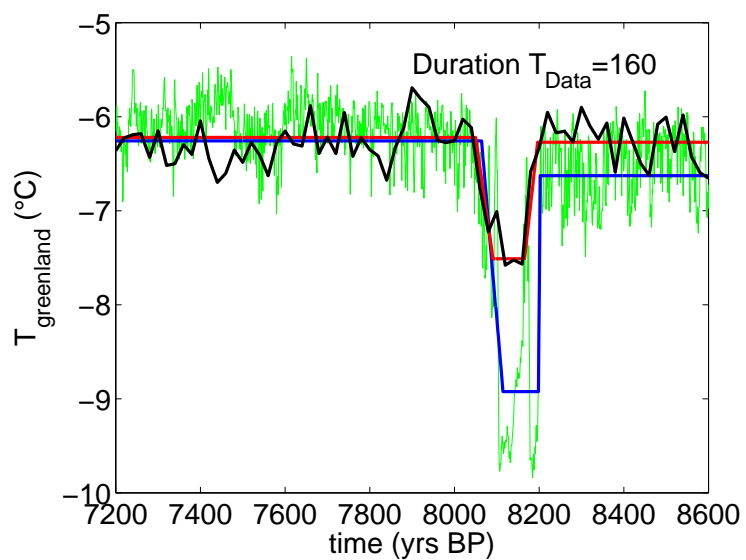


Figure 2.3: (black) The Kriging Mean of the Greenland ice core data (in $\delta^{18}\text{O}_{\text{ice}}$ / offset to be displayed together with CLIMBER-2.3 output), (green) example CLIMBER-2.3 output of the cold event with added weather noise, (red) trapezoid fit to Greenland data, (blue) trapezoid fit to CLIMBER-2.3 output

2.2.2 CLIMBER-2.3

In this study the climate model CLIMBER-2 version 3 is employed. CLIMBER-2.3 (CLIMate-BiospERe model) is a 2.5-dimensional, low resolution climate system model designed for simulation of large-scale processes on time scales from seasonal to millenia and longer [Petoukhov et al. (2000)]. The model is classified as model of intermediate complexity (EMIC) between simple one- or two-dimensional models on the one hand and complex 3-D climate GCMs on the other. It consists of modules describing atmosphere, ocean, sea ice, land surface processes, terrestrial vegetation cover and the global carbon cycle. CLIMBER-2.3 only has a coarse spatial resolution. Orography and bathymetry are systematically resolved and the model describes only the large-scale patterns of the dynamics with daily time steps. The atmosphere module is a dynamical-statistical 2.5-dimensional atmosphere model as the vertical structure of the atmosphere and the synoptic-scale activity are parameterized. For atmosphere and land modules the latitudinal resolution is the same (10°). Atmosphere and land modules consist of seven equal longitudinal sectors of 51° . In the atmosphere model, the dynamical properties are determined on ten uneven vertical levels. The radiation schemes account for stratus and cumulus clouds, water vapor, carbon dioxide and aerosols. Radiative fluxes are computed on 16 vertical levels. The ocean component is similar to the ocean module employed by [Schmittner and Weaver (2001)] as both originate from the module by Wright and Stocker (1991). It uses 20 uneven vertical layers and three longitudinal ocean boxes (Atlantic, Indic, Pacific) and has a latitudinal resolution of 2.5° . The ocean module computes distributions of temperature, salinity and meridional and vertical velocity components. The submodels are coupled interactively without flux adjustments through fluxes of heat and water and momentum is transferred from the atmosphere to the ocean. CLIMBER-2 has been validated in various ways. The simulated climate characteristics of the atmosphere and the ocean for the preindustrial climate state agree well with observational data [Petoukhov et al. (2000)]. Several sensitivity studies have been performed [Ganopolski et al. (2001)] to compare the model response to changes in solar insolation, carbon dioxide, freshwater flux and land cover with results of GCMs. The model response, eg. to a CO_2 concentration increase, qualitatively agrees with results of GCMs. A third possible method of validation is the comparison of model output to paleoclimatic data. Driven by natural and anthropogenic forcings, the temperature variations of the last millennium were reproduced [Bauer et al. (2003)]. Many aspects of glacial (21 kyrs BP) and mid-Holocene (6 kyrs BP) climate seen in paleo-data have successfully been reproduced [Ganopolski et al. (1998)]. Even abrupt climate changes can be reproduced [Ganopolski and Rahmstorf (2001)].

Bauer et al. (2004) used CLIMBER-2 with different forcing mechanisms including noisy freshwater fluxes to reproduce a cold event in a climate state corresponding to early Holocene conditions around 9 kyr BP. By applying a freshwater pulse

2 Theory & Methodology

combined with additional freshwater noise and different baseline freshwater fluxes to the northern Atlantic basin Bauer et al. (2004) were able to lengthen the duration of the cold event to a centennial scale.

The low computational costs of CLIMBER-2.3 allows the creation of huge ensemble climate scenarios necessary for the ensemble operationalization of a Bayesian approach (see section 1.2). The CLIMBER-2.3 model was used by von Deimling et al. (2006) in this way to constrain eleven internal parameters which are most influential on Climate Sensitivity. The learning effect was transformed to Climate Sensitivity, to a range similar to the IPCC estimate and thereby ruled out much higher estimates from other simulations.

2.2.3 Methodology of model-data intercomparison

For establishing the likelihood of the parameters α in question, namely the ocean diffusivities, the output of the CLIMBER-2.3 simulations of the 8.2 ka event are compared to the Greenland ice core records of this period. This approach requires the following assumptions: (1) For being comparable in principal, the model output and paleo-data under consideration need to cover the same spatial and temporal domain. (2) The ‘statements’ under comparison should be of the same type, which means in physical applications that the compared data should be on the same quantity (that is in the same unit) and both parts should originate from the same process. The second part is the analog of the assumption that the model in use is capable in principal of reproducing the important features of the data from the natural system.

To fulfill condition (1) the paleo-data of different locations in Greenland are aggregated to CLIMBER-2.3 box scale (i), whereas the CLIMBER-2.3 output is aggregated to 20 year resolution (ii). With respect to condition (2), two objections occur: While the paleo-data contain $\delta^{18}\text{O}_{\text{ice}}$ time series, CLIMBER-2.3 projections are in terms of temperature. Furthermore the observations are obscured by local weather noise not represented by the noise η in CLIMBER-2.3n. Therefore a transformation $\delta^{18}\text{O}_{\text{ice}} \mapsto T$ has to be found for the Greenland temperature T_{grl} (aggregated to CLIMBER-2.3 box scale) (iii). Finally a noise model is implemented to account for the local weather noise in the Greenland paleo-signal (iv).

(i) Aggregation of paleo proxy data to CLIMBER box scale

For comparison to the CLIMBER-2.3n output, the proxy data from the different measurement locations are aggregated to the CLIMBER-2.3 box scale by Kriging their mean. Following [Wackernagel (1995)] it is assumed that the data samples $z(\mathbf{x}_\alpha)$ for each timestep (in this case z denotes $\delta^{18}\text{O}_{\text{ice}}$, \mathbf{x}_α denoting the place sample α is taken at) are realizations of identically distributed random variables $Z(\mathbf{x}_\alpha)$. This assumption holds after long term trends are removed from the data

with a running mean filter.

As the timeseries of proxy data are taken at irregular spacing in the CLIMBER-2.3 box of interest, one is interested in estimating the mean m over the box. To take into account the spatial correlation structure of the data a weighted mean is used:

$$M^* = \sum_{\alpha=1}^n w_{\alpha} Z(\mathbf{x}_{\alpha}), \quad (2.9)$$

with n different proxy locations. The weights w_{α} are determined by minimizing the variance of the estimation error

$$\text{var}(M^* - m) = \sum_{\alpha=1}^n \sum_{\beta=1}^n w_{\alpha} w_{\beta} C(\mathbf{x}_{\alpha} - \mathbf{x}_{\beta}) \quad (2.10)$$

under the unbiasedness condition

$$\sum_{\alpha=1}^n w_{\alpha} = 1. \quad (2.11)$$

The variance of the estimation error contains the covariance function $C(\mathbf{h})$ which is defined via

$$C(\mathbf{h}) = \text{cov}(Z(\mathbf{x}), Z(\mathbf{x} + \mathbf{h})). \quad (2.12)$$

The minimization is computed by introducing the condition on the weights by the method of Lagrange, defining an objective function ϕ , containing the quadratic function and a term containing a Lagrange multiplier μ :

$$\phi(w_{\alpha}, \mu) = \text{var}(M^* - m) - 2\mu \left(\sum_{\alpha=1}^n w_{\alpha} - 1 \right) \quad (2.13)$$

and setting the partial derivatives of the objective function to zero. One ends up with solving a system of $n + 1$ linear equations for the optimal weights w_{α}^{KM} :

$$\begin{cases} \sum_{\beta=1}^n w_{\beta}^{KM} C(\mathbf{x}_{\alpha} - \mathbf{x}_{\beta}) - \mu_{KM} = 0 & \text{for } \alpha = 1, \dots, n \\ \sum_{\beta=1}^n w_{\beta}^{KM} = 1, \end{cases} \quad (2.14)$$

Or, written as matrix equation:

$$\begin{pmatrix} C(\mathbf{x}_1 - \mathbf{x}_1) & C(\mathbf{x}_1 - \mathbf{x}_2) & \dots & C(\mathbf{x}_1 - \mathbf{x}_n) & -3 \\ C(\mathbf{x}_2 - \mathbf{x}_1) & C(\mathbf{x}_2 - \mathbf{x}_2) & \dots & C(\mathbf{x}_2 - \mathbf{x}_n) & -3 \\ \vdots & \vdots & \ddots & \vdots & \vdots \\ C(\mathbf{x}_n - \mathbf{x}_1) & C(\mathbf{x}_n - \mathbf{x}_2) & \dots & C(\mathbf{x}_n - \mathbf{x}_n) & -3 \\ 1 & 1 & \dots & 1 & 0 \end{pmatrix} \cdot \begin{pmatrix} w_1^{KM} \\ w_2^{KM} \\ \vdots \\ w_n^{KM} \\ \mu^{KM} \end{pmatrix} = \begin{pmatrix} 0 \\ 0 \\ \vdots \\ 0 \\ 1 \end{pmatrix} \quad (2.15)$$

2 Theory & Methodology

of the form $\mathbf{A} x = b$, which can directly be solved by inversion to $x = \mathbf{A}^{-1}b$. The minimal estimation variance σ_{KM}^2 is computed by using equation (2.10) for the optimal weights and shows up to be given by the Lagrangian multiplier, $\sigma_{KM}^2 = \mu_{KM}$. Applying this procedure independently for each timestep one ends up with the estimate for the mean Greenland value of $\delta^{18}\text{O}_{\text{ice}}$ on the CLIMBER-2.3 box scale $M^*(t)$.

(ii)&(iii) Time resolution and temperature transfer function

The transformation of $\delta^{18}\text{O}_{\text{ice}}$ data to temperature values has been done for single boreholes in various ways [Johnsen et al. (1995), Cuffey and Clow (1997), Dahl-Jensen et al. (1998), Johnsen et al. (2001)]. Depending on the method employed the average dropping by 1.5 ‰ in $\delta^{18}\text{O}_{\text{ice}}$ during the 8.2 ka event corresponds to a surface air temperature drop of (3 – 6) K [Bauer et al. (2004)]. As there exists no Greenland-wide transfer function and the existing ones for single borehole data bare an uncertainty of factor 2-4, an alternative scheme for the model-data comparison is presented here. Instead of directly transferring the Greenland time series to CLIMBER-2.3 output and thereby contaminating data y with the uncertainties from the transfer functions a nonlinear mapping is introduced that projects both the CLIMBER-2.3 output and the Greenland paleo-data (y) to a quantity T with one common unit. In this study this quantity is chosen to be the duration of the 8.2 ka event. This duration T is measured by fitting a trapezoid function to the output y in a Least Square Fit (see figure 2.2.1). The low dimension of T (i.e. ‘1’) being the duration of the cold event is beneficial for the Bayesian Learning scheme (as seen in section on Bayesian Learning). The aggregation of the CLIMBER-2.3 output to the sampling resolution of the paleo-data can be done after this projection by binning the different durations with an appropriate resolution (limited by the time resolution of the paleo-data). Using this scheme, only one point remains at which a $\delta^{18}\text{O}_{\text{ice}}$ value needs to be transferred to temperature. This is the amplitude of the weather noise which is to be applied to the CLIMBER-2.3 output to fulfill the comparability condition (see below).

(iv) Applying weather noise to CLIMBER-2.3 output

To meet condition (2), that is to ensure the comparability of CLIMBER-2.3 output to Greenland paleo-data, the model output has to be adapted to the data by applying local weather noise², not represented in the CLIMBER-2.3 output up to now. In this study an additive weather noise model ζ is suggested. The CLIMBER-2.3 output is modified in the way: $y' \rightarrow y := y' + \zeta$, where ζ is drawn *iid* from a normal distribution $N(0, \sigma)$. The noise amplitude σ is transferred from the observable weather noise in Greenland which is in terms of $\delta^{18}\text{O}_{\text{ice}}$ derived

²Hereby denoting the fraction of variability that does not correlate with ocean variability.

from the covariance of the different data stations in Greenland to σ in units of T via $\sigma^2 = x^2 \cdot \sigma_{\text{weather}}^2$ constrained by the following assumption:

$$\frac{\sigma_{\text{weather}}^2}{(\text{var}(\delta^{18}\text{O}_{\text{ice}}) - \sigma_{\text{weather}}^2)} = \frac{x^2 \cdot \sigma_{\text{weather}}^2}{\text{var}(y')}, \quad (2.16)$$

with y' the stationary CLIMBER-2.3 output, $\delta^{18}\text{O}_{\text{ice}}$ the stationary (without long term trends) Greenland data, x the transfer factor from $\delta^{18}\text{O}_{\text{ice}}$ to temperature (under the assumption of a simple linear transfer function). The main assumption of this transformation is that noise-driven CLIMBER-2.3 has all the necessary variability beyond weather, reddened³ by ocean dynamics.

That means the proportion of weather noise to the variance of the timeseries without weather noise should be the same in the model output and the data. The difference in the Greenland data on short time scales (after long term trends are removed) should only originate from local weather noise. So the amplitude of this Greenland weather noise σ_{weather} can be derived as variance from the Kriging of the Greenland ice core data. Hereby it is important not only to transfer σ in unit but also to rescale the amplitude properly according to the different time resolutions Δt in data and model output [Kleinen et al. (2003)]:

$$\frac{\sigma_{\Delta t}}{\sqrt{\Delta t}} = \frac{\sigma_{\Delta t'}}{\sqrt{\Delta t'}}. \quad (2.17)$$

Therefore using σ_{weather} and equation (2.17) the transfer parameter x is tuned to fulfill (2.16). The resulting time series σ can either be directly applied to the CLIMBER-2.3 output for each timestep, or one takes only the mean of σ as a global amplitude.

³While for white noise the amplitude is generated by a normal distribution for each single timestep, red noise contains a memory of amplitude of distortion from earlier time steps.

2 Theory & Methodology

3 Simulation experiments

3.1 The 8.2 ka event in CLIMBER-2.3

3.1.1 Experimental setup

Following Bauer et al. (2004) the transient climate simulations for the 8.2 ka event are started from a near equilibrium state adapted to the boundary conditions for 9 ka BP. These are the orbital parameters affecting solar irradiance (eccentricity, obliquity, and precession) [Berger (1978)], the atmospheric CO₂ concentration of 261 ppm and a remnant Laurentide ice sheet on the North American continent [Marshall and Clarke (1999)]. The resulting 9 ka climate state is characterized by nearly the same global and hemispherical temperatures in the annual mean as in the preindustrial state with 280 ppm but the seasonal temperature cycle is stronger than in the preindustrial state. For a detailed comparison of the 9 ka state to the preindustrial state in CLIMBER-2.3 see [Bauer et al. (2004)]. For reaching this equilibrium state a 3 ka equilibrium run was performed for each parameter setting (see sampling strategy) under the 9 ka boundary conditions. Within this time the important climate characteristics representing the longer ocean time scales (e.g. the volume averaged ocean temperature) reach near equilibrium. These equilibrium states were saved and the 8.2 ka simulations are then restarted from this state. This allows a large number of simulations per parameter setting without the need of reaching equilibrium each time.

In this restarted simulation runs, the cold event is initialized at 8200 yrs BP (that is after 800 model years) by a freshwater pulse released to the northern Atlantic Ocean (as done by Bauer et al. (2004)), that are the ocean grid cells from 50-70° N in CLIMBER-2.3, representing a pulse-like drainage of melt water from the Lake Agassiz through Hudson Bay as suggested by Teller et al. (2002) and Leverington et al. (2002). This pulse has a volume of $1.6 \times 10^{14} \text{m}^3$ and was released (in CLIMBER-2.3) within two years; that corresponds to a freshwater flux of 2.6 Sv.

As Bauer et al. (2004) showed, the total duration of the cold phase resulting from this setting (around 70 yrs) is much shorter than inferred from the reconstructed data. To overcome this discrepancy and to account for short term variability in the runoff associated with the melting of the Laurentic Ice Shield (LIS) and for a possible enhanced runoff through St. Lawrence River prior to the 8.2 ka event, originating from the ongoing melting of the LIS or from the overflow of pro glacial

3 Simulation experiments

lakes, a noise model and a baseline flux are added to the surface freshwater fluxes computed by the model. The noise is generated by a white noise model with variable standard deviation (σ) and a different seed for the noise generator is chosen for each realization of a simulation with a certain setting of parameters. Bauer et al. (2004) showed that by including this noise, the model output strongly depends on a certain realization of the noise. Thus this noisy version of the 8.2 ka event in CLIMBER-2.3 requires an ensemble approach to estimate the influence of the different parameters as the nonlinearity of CLIMBER-2.3 especially during the 8.2 ka event strongly changes the influence of a parameter setting on the model output. The resulting freshwater forcing for one realization of the 8.2 ka scenario is shown in figure 4.1. Running the 8.2 ka scenario several hundred times and considering only one aspect of the cold event (e.g. the duration, the temperature change) one ends up with a histogram of this aspect of the event which represents an experimental probability distribution function over the given aspect.

The additional baseline flux represents enhanced runoff from the two possible runoff routes: Hudson Bay and St.Lawrence strait. In CLIMBER-2.3 these routes are represented by introducing additional fluxes in the Atlantic grid cells between (50-70) $^{\circ}$ N (Hudson) and (40-50) $^{\circ}$ N (St.Lawrence). There exist different estimates for the strength and the duration of these additional fluxes [Teller et al. (2002), Clark (2001)]. For reasons of simplicity, that means reduction of dimensions, in this study only one additional baseline flux is introduced. As Bauer et al. (2004) showed, such an additional baseline can prolong the duration of the cold event considerably. The baseline flux can alter in duration and strength and the noise may vary in amplitude. So the experimental setup of the 8.2 ka simulation introduces at least three additional uncertain parameters to deal with.

3.1.2 Sampling strategy

Different model intrinsic parameters vary in their influence on the model performance in the 8.2 ka event. Thus two parameters of major influence on the 8.2 ka event were chosen for the Bayesian Learning step. Out of the 11-dimensional parameter space investigated by von Deimling et al. (2006) the horizontal and vertical ocean diffusivity were chosen under the working hypothesis, that these two parameters are most influential on the climate signal from Greenland and therefore also for the 8.2 ka event. Hence a large reduction in the space of consistent parameter combinations of diffusivities can be suspected from the model-data intercomparison. Before the Bayesian Learning can be applied, one has to gather the prior knowledge about the parameters under consideration. The most conservative constraints on the diffusivities are given as an expert knowledge by the constructors of CLIMBER-2.3 as follows (see von Deimling et al. (2006)): The horizontal diffusivity $k_H = 200-5000$ {std. = 2000} m^2/s is directly addressed by the CLIMBER-2.3 variable *AHOC*. The vertical diffusivity is taken to follow a verti-

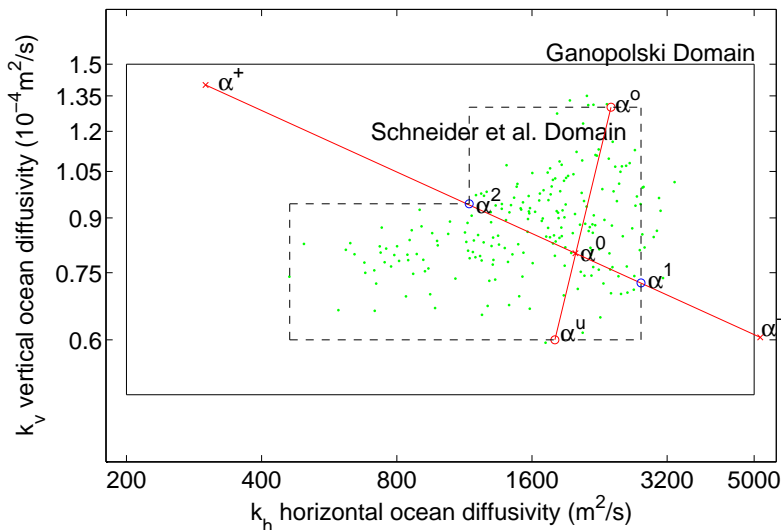


Figure 3.1: two-dimensional parameter space of ocean diffusivities with different constraints

cal profile after Bryan Lewis with $k_V = 0.1-1.0 \times 10^{-4}$ {std. = 0.3×10^{-4} } m^2/s at top, $0.5-1.5 \times 10^{-4}$ {std. = 0.8×10^{-4} } m^2/s at the profile's turning point and $1.1-2.0 \times 10^{-4}$ {std. = 1.3×10^{-4} } m^2/s at ocean bottom. The CLIMBER-2.3 variable a_Kv addresses the diffusivity at the turning point of the profile. These first constraints to the diffusivities reflect the space of physically reasonable values for the diffusivities. In the present study this space is called the *Ganopolski Domain*. As a second step of including prior knowledge the insights of [von Deimling et al. (2006)] are used. He applied constraints on the present day performance of the model to reduce uncertainty of 11 model parameters (including the ocean diffusivities). Following this approach an ensemble of 1000 members is created according to a Monte Carlo scheme. Each model realization only differs in the choice of the ocean diffusivities. The values for $AHOC$ and A_Kv are sampled on a logarithmic scale according to a beta distribution within the bounds of the Ganopolski Domain. For each ensemble member an equilibrium run of 3000 years is performed under the boundary conditions of present day climate. Seven of the resulting climate characteristics are constrained by a set of boundaries used by von Deimling et al. (2006) to represent tolerable present day climate states, containing intervals for the annual mean values which encompass corresponding empirical estimates:

- global SAT 13.1-14.1 °C [Jones et al. (1999)]
- area of sea ice in the Northern Hemisphere IN 6-14 mil km^2 and in the Southern Hemisphere IS 6-18 mil km^2 [Cavalieri et al. (2003)]

3 Simulation experiments

- total precipitation rate PRC 2.45-3.05 mm/day [Legates (1995)]
- maximum Atlantic northward heat transport FATMX 0.5-1.5 PW [Ganachaud and Wunsch (2003)]
- maximum of North Atlantic meridional overturning stream function NADW 15-25 Sv [Talley et al. (2003)]
- volume averaged ocean temperature TV 3-5 °C [Levitus 1982]

In figure 3.1.2 the parameter settings that pass all seven constraints are indicated by green dots. Under the assumption that each of the constraints leaves over areas of parameter values that are simply connected, the leftovers of all seven constraints also constitute a simply connected domain, here called *Present Day*- or *Schneider Domain*. This study now aims at a reduction of the boundaries of the diffusivities with respect not only to the Ganopolski- but also to the Schneider Domain.

As the construction of the likelihood for each parameter setting in all five dimensions (the diffusivities, the noise amplitude, the duration and strength of the baseline flux) requires several hundred runs of the 8.2 ka simulation it is impossible to screen the Schneider Domain completely with a factorial design. Therefore another approach is used here: Backed by numerical results the likelihood is assumed to be of normal form in each dimension, that means the domain of appropriate parameters is a multi-dimensional ellipsoid, it is suitable to sample only a few points in each dimension with all other parameters unchanged. From this one gets the point of maximum likelihood. Starting from this point of maximum likelihood one defines the uncertainties in each dimension by looking for the point where the likelihood has fallen to the $1/e$'s fraction¹. These boundaries are projections of the ellipsoid describing the multi-dimensional error bar onto the single dimensions, they are used to fit the likelihood-ellipsoid to the data. Once one has the complete ellipsoid, the *real* uncertainty with respect to any dimension can be computed.

Within the two-dimensional subdomain of the ocean diffusivities (k_H, k_V) the samples are taken along the line (in log space) between the parameters α^- , α^0 and α^+ . This follows the construction of a parameter α out of the diffusivities which is most influential on the Atlantic overturning stream function and therefore most likely also on the 8.2 ka event as done by Held and Kleinen (2004). To cover two dimensions, samples are also taken along the direction nearly orthogonal to α . With this approach the assumption of the major influence of α can be tested.

¹When working with the likelihood alone, rather than with the product of prior and likelihood, as required by Bayesian Theory one loses interpretation of a probability measure, however gains objectivity. Then various choices of likelihood ratio are possible.

3.2 Summary

The model setup for simulation of the 8.2 ka event with CLIMBER-2.3n (the noisy version of CLIMBER-2.3) has been presented. The experiment related tuning parameters concern the freshwater forcing that shows responsible for the timing and duration of the cold event as seen in the Greenland temperature output: The duration and strength of a baseline flux added to the also uncertain North American continental runoff and the amplitude of additional white noise perturbing the North Atlantic freshwater forcing. The parameters representing horizontal and vertical ocean diffusivity were chosen as uncertain parameters to be addressed by the Bayesian Learning scheme under the assumption of their major influence on the model's performance at 8.2 ka. A sampling strategy has been provided to Bayesian learn existing prior knowledge on the diffusivities and to estimate the high-dimensional likelihood function with a multi-Gaussian approach.

3 Simulation experiments

4 Results & Interpretation

In this chapter the results of the 8.2 ka event simulations are presented and interpreted starting with an overview of the reproduced 8.2 ka climate state in section 4.1. The dependency of the cold event duration T on the realization of freshwater noise makes an ensemble approach necessary. The resulting histogram of durations is presented and discussed in section 4.2. In section 4.3 the Bayesian Learning step is carried out in detail and the resulting learning effect is transferred to other climate parameters in section 4.4. The results are summarized in section 4.5.

4.1 Interpretation of the 8.2 ka event in CLIMBER-2.3

The simulation of the 8.2 ka event discussed below is performed according to the experimental setup described in section 3.1.1. Starting from the equilibrium state adapted to the boundary conditions of 9 ka BP a freshwater forcing is applied consisting of a baseline flux with an amplitude of $\text{RFWFBG}=0.03$ Sv and a duration of 1000 yrs with additional white noise of amplitude $\sigma = 0.03$ Sv and a freshwater pulse of 2.6 Sv after 800 yrs. The freshwater forcing is applied to the northern Atlantic region (50-70°N). Time series of some aggregated climate variables for this 8.2 ka event simulation are shown in figure 4.1, the fields of meridional stream function, potential density and frequency of convection events are shown in figures 4.2-4.4 both before and during the cold event.

The left column represents the state of the northern Atlantic ocean before the pulse is applied. The well known North Atlantic conveyor belt is well represented in the meridional stream function. The relatively warm and saline water is transported north by the near surface North Atlantic current. The potential density $\rho = f(T, S)$ (4.3) that depends on temperature and salinity shows an instability as the isolines proceed vertically, thus downward convection takes place. The water sinks down at the Iceland-Greenland ridge and flows southward in a vertically and horizontally broad current as North Atlantic Deep Water. Normally, that means in the standard Holocene setting denoted as ON mode of the North Atlantic Overturning Circulation, the maximum of this circulation is located slightly north of the Iceland-Greenland ridge at a depth of about 1000 m.

At 8.2 ka BP an enormous amount of freshwater is released into the surface layer of the northern Atlantic (4.1(a)). Due to its lower salinity the potential density of

4 Results & Interpretation

this freshwater is lower than in the deeper ocean, thus the water column becomes stable (4.3(r)) and the downward convection stops immediately. As the northward transport of warm saline water does not stop, the overturning is not turned off completely but shifted southward; the warm water now sinks at a latitude of 40-50°N (see 4.2(r)). This slowing down of the overturning circulation was shown with an equilibrium setup by Bauer et al. (2004) and is now also seen in a transient model run. This state of weakened overturning circulation (maximum of 12 Sv (see figure 4.2(r))) is called intermediate (INT) as it lies in between of the ON mode with a maximum in overturning of 18 Sv and the glacial OFF mode without overturning. The output field containing the frequency of convection events (4.4) allows a clear separation between the ON, the INT and the OFF mode. In the ON state, convection takes place from the surface to the deep ocean along the slopes of the Iceland-Greenland ridge. In the INT state the convection is shifted south and consists of a purely wind driven part at the surface and a slowed overturning that reaches only 500 m downwards. The OFF mode only shows the wind driven surface current without any convection events (not shown). The stability and characteristics of this INT mode were also investigated by Bauer et al. (2004). As the overturning is weakened at 8.2 ka BP (4.1(b)), the northward heat transport is also shortened and thus the temperature in the northern hemisphere decreases whereas the southern hemisphere becomes warmer (4.1(f)) due to the so called seesaw effect [Crowley (1992)]. The cooling is seen strongest in the North Atlantic region (about 5° C in Greenland temperature (4.1(c))). The cooling corresponds to lesser precipitation (4.1(e)). In this example the cold period lasts about 250 years.

4.2 The histogram of cold event duration

The model's performance strongly varies for different realizations of freshwater noise. As pointed out in section 3.1.1 this demands an ensemble approach to investigate the influence of model parameters on the model's performance around the 8.2 ka event. For each parameter setting the event was simulated 150-300 times to fit the error condition (see equation (2.8)). For reasons of simplicity and computational feasibility, the model output and the ice core data were projected onto the duration T of the cold phase. T was estimated by a nonlinear trapezoid fit (as described in section 2.2.3) and binned into boxes of bin-size 20 years (according to the uncertainty of the Greenland ice core data). The resulting histogram represents the relative frequency of occurrence of different cold event durations (example see figure 4.5). Surprisingly the histogram reveals a system of at least two different modes of duration; one short mode around 80 years and a longer mode centered about 30 years after the termination of the additional baseline flux used in the experiment. This points to coexisting physical mechanisms as origin for the modes. Sensitivity analysis on the duration of baseline flux

4.2 The histogram of cold event duration

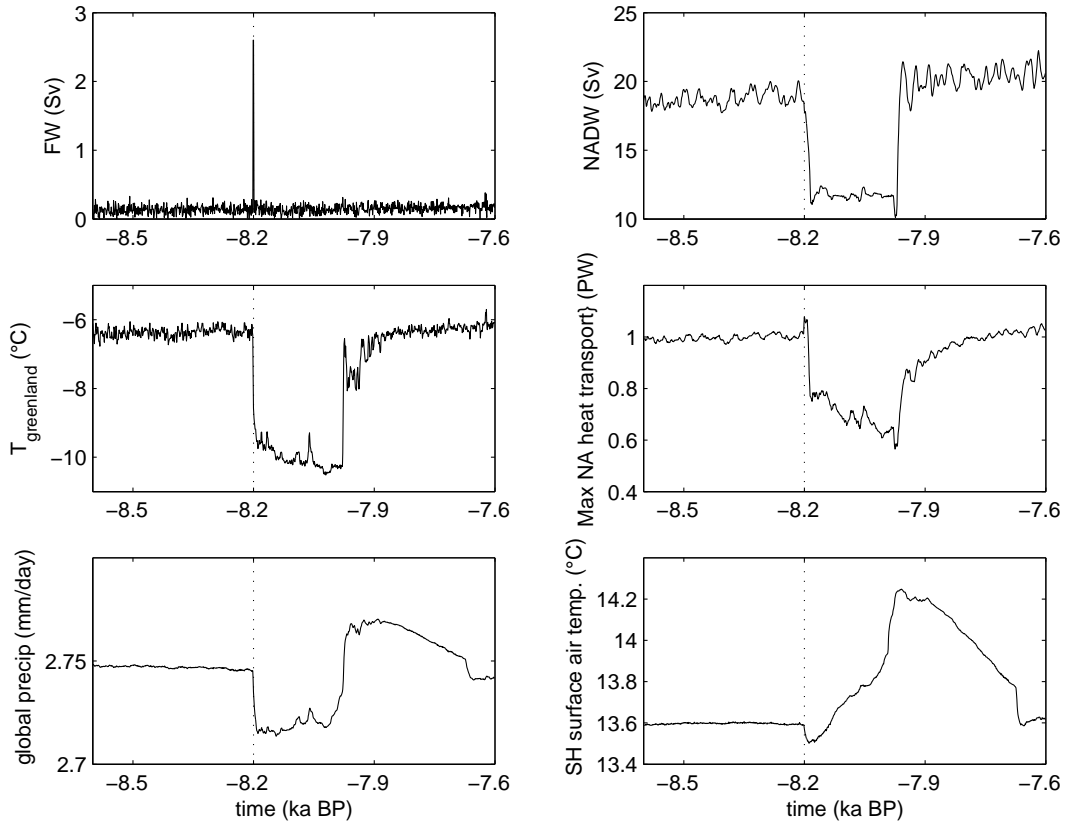


Figure 4.1: Time series of various climate variables for one realization of an 8.2 ka event simulation, showing (a) the composite freshwater forcing, (b) the NADW formation rate, (c) the temperature in Greenland [a composite of several boxes], (d) the maximum Atlantic northward heat transport, (e) global precipitation and (f) the southern hemispheric surface air temperature

4 Results & Interpretation

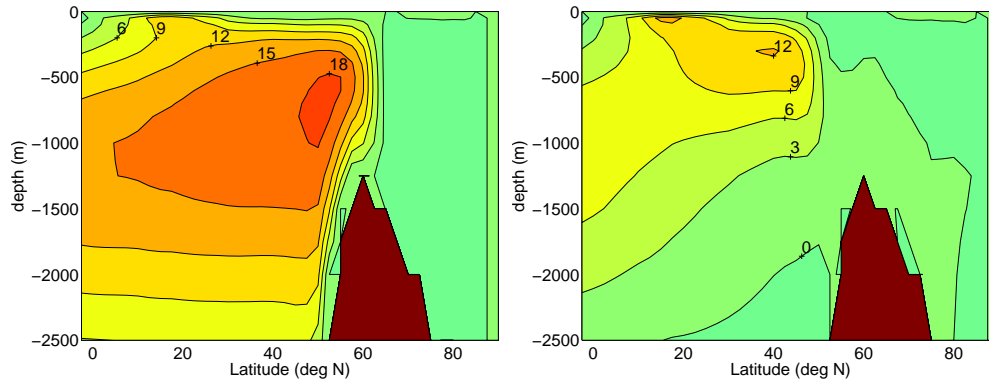


Figure 4.2: Atlantic meridional stream function in Sv of ON (left) and INT (right) state in transient 8.2 ka event simulation. Isolines are in steps of 3 Sv.

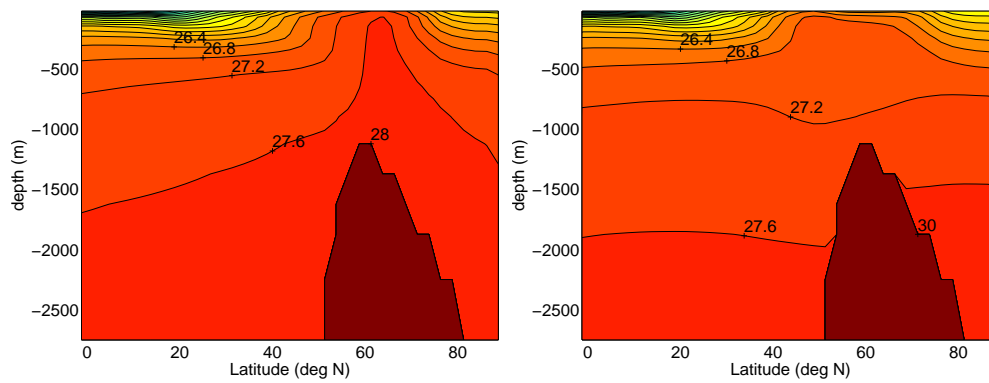


Figure 4.3: Potential density of ON (left) and INT (right) state in transient 8.2 ka event simulation in kgm^{-3} above 10^3kgm^{-3} with isolines in steps of 0.4kgm^{-3} .

4.2 The histogram of cold event duration

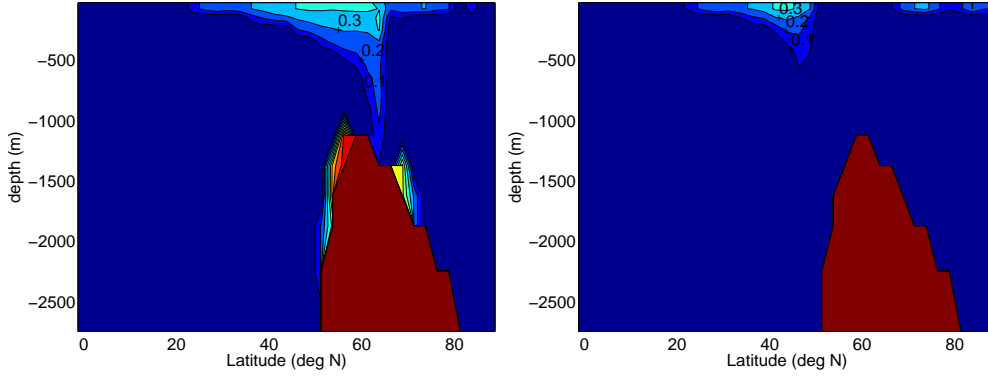


Figure 4.4: Frequency of occurrence of convection events of ON (left) and INT (right) state in transient 8.2 ka event simulation with isolines in steps of 0.1.

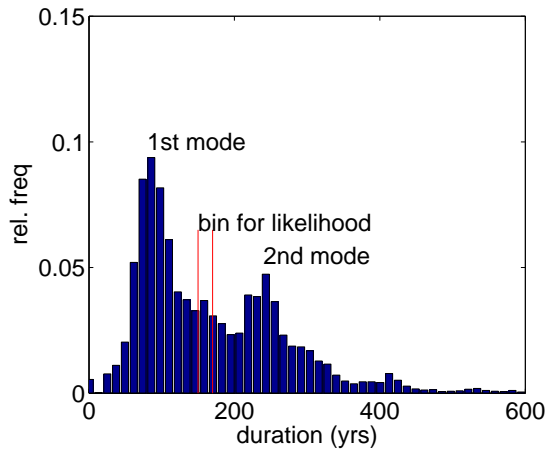


Figure 4.5: Histogram of durations T of the cold event for different realizations of noise η ; parameter setting: $a_{\text{hoc}} = 2000 \text{ m}^2/\text{s}$, $a_v = 0.8 \cdot 10^{-4} \text{ m}^2/\text{s}$, $\sigma_{\text{noise}} = 0.06 \text{ Sv}$, $D_{\text{baseline}} = 1000 \text{ yrs}$

4 Results & Interpretation

for a given strength and vice versa have been performed. Figure 4.6 shows the histograms of durations T of the 8.2 ka cold event for different values of duration D of baseline flux with all other parameters kept constant. The duration D of baseline flux shows strong influence on the histogram of cold event durations, as it moves the second mode according to the duration $D + 30$ years. In this case the first mode vanishes for longer durations D . In another sensitivity study without any additional baseline the second mode vanishes and the first mode shows only weak dependence on the strength of background freshwater runoff (without figure). These findings might be explained as follows: The short mode represents the mean lifetime of the INT state of overturning circulation which is not altered considerably by different values of freshwater strength (without figure) unless the baseline gets strong enough to completely shut down the circulation as happened in the lower cases in figure 4.5 due to the high freshwater rate of 0.06 Sv introduced for longer than 800 years.

The second mode is clearly triggered by the termination of the baseline flux. One suggestion for a physical interpretation is that actually in the second mode it is not the INT but the OFF mode that is reached by the freshwater forcing. By comparing the overturning stream function for runs lying inside the first and second mode this explanation was ruled out. It seems clear that a continuing inflow of freshwater keeps the overturning from recovering as it smoothes the gradient in density. Nevertheless the concrete physical mechanism behind the second mode stays an open question and should be addressed in further studies.

The first mode centered around 80 years represents a centennial time scale characteristic for advective processes impacting the whole Atlantic (from time scale analysis). The characteristic time scale for the decay of regional distortions only reaches from annual to decadal scales and the diffusive scale of the Atlantic reaches 1000 years. This comparison points to an at least hemispherical impact of the 8.2 ka event in CLIMBER-2.3.

Besides the resulting mean of cold event duration in mode one is too short by factor 2 compared to the Greenland ice core data. As this mode was not to be altered by adjusting the experiment related parameters it follows that the single-pulse scenario in CLIMBER-2.3 is not able to produce sensible high likelihood for a duration of 160 years without additional baseline flux. This leads to different possible conclusions: Under the assumption that nature has realized a highly probable state during the 8.2 ka event this means that either the model setting is in general unable to realistically represent the 8.2 ka event or if not so the one-pulse scenario can only lead to a high likelihood by introducing additional baseline fluxes (as done in this experiment). As an alternative one would have to consider a multi-pulse scenario. Although the forcing used here leads to an interesting intermediate (or exited) mode of THC with a timescale indicating at least hemispherical range of the event the physical mechanism(s) behind this time scale remain(s) open to further studies.

Nevertheless the Bayesian approach is capable of providing the likelihood of the

4.3 Constructing the likelihood

parameter setting in question by adding up the relative frequencies of durations T that lie inside the interval of $T = (160 \pm 10)$ yrs. Thus the Bayesian approach formally is in no need for physical interpretation as it simply assimilates data in a coherent scheme. The corresponding conditional likelihood

$$P(T = (160 \pm 10) \text{ yrs} | \alpha = [a_{\text{hoc}} = 2000, a_v = 0.8 \cdot 10^{-4}, \text{AN} = 0.03, \text{FW} = 0.06, D])$$

in figure 4.6 (right) shows, that with the given parameter setting the right duration of cooling can best be achieved with a duration D of baseline flux near 860 years (maximum of conditional likelihood) with an error bar lc , defined as the $1/e$ likelihood contour reaching from 790 to 930 years. So the experiment-related parameters defining the baseline flux have a strong influence on the shape of the histogram and therefore on the likelihood of ocean diffusivities.

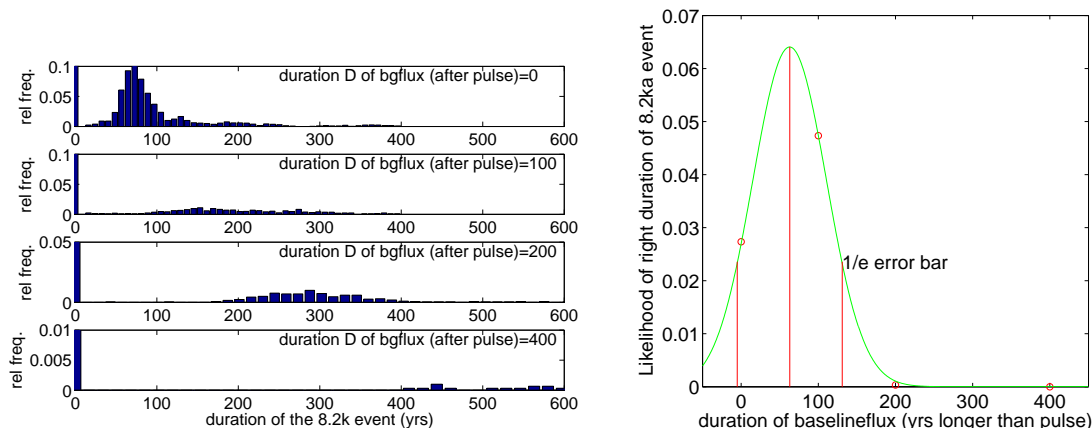


Figure 4.6: (left) histograms for different durations of baseline flux, (right) corresponding conditional likelihood of right duration of the 8.2 ka event (160 ± 10 yrs) given the parameter setting

4.3 Constructing the likelihood

Constructing the likelihood $P((T = 160 \pm 10) \text{ yrs} | \alpha)$ one has to keep in mind, that the duration of the cold event around 8.2 ka BP in CLIMBER-2.3 simulations may not only depend on the ocean diffusivity parameters a_{hoc} and a_v (denoted $^1\alpha$, $^2\alpha$) alone but on additional model parameters (e.g. experiment-related parameters like amplitude of noise, duration and strength of baseline freshwater flux, denoted $^3\alpha$ - $^5\alpha$ or on other model parameters like the height of stratiform clouds etc.). These additional uncertain parameters add to the complexity of the problem by enlarging the dimension of α . This problem is handled by an iterative approach.

4 Results & Interpretation

Firstly the conditional probability of the diffusivities is computed by assuming all the other parameters to be known exactly (section 4.3.1). Although this is not true it reduces the dimension of the problem and allows to estimate the learning effect on the diffusivities alone. The Bayesian approach then permits to improve the result according to the multi-dimensional Gaussian approach pointed out in section 3.1.2 by including additional model runs which vary in the other dimensions of parameter vector α (section 5.2).

4.3.1 Conditional likelihood of ocean diffusivity parameters a_{hoc} and a_v

For this first step the ocean diffusivities were tuned within a square domain made up by $\alpha_{1,u,2,o}$ of the Schneider Domain (see figures 4.7 & 3.1.2). For each of the parameter settings 150 8.2 ka model simulation runs have been performed and the corresponding likelihood was computed according to equation (2.5). All other model parameters were kept constant at the standard values. The experiment related parameters were also chosen to be known constants: The amplitude of freshwater noise σ was estimated from [Walsh and Portis (1999)] who delivered estimates for the variance of fluctuations in northern Atlantic freshwater budget from evaporation and precipitation. Rescaled to the North Atlantic region in CLIMBER-2.3 this corresponds to a variance of $\sigma = 0.02$ Sv. As the fluctuations in freshwater runoff and sea ice melting have to be included the amplitude of noise was chosen as $\sigma = 0.05$ Sv. Duration and strength of the additional freshwater baseline were chosen as $D = 900$ yrs and $FW = 0.03$ Sv. These represent the personal knowledge of the author about optimal choice of the experiment related parameters gained by single dimension sensitivity experiments. Later on this choice has to be replaced by a more systematic approach (see section 5.2).

The resulting data of empirical conditional likelihood are well represented by a two-dimensional Gaussian Least Square Fit (shown in figure 4.7(left)). The half-width of the Gaussian is displayed as a divisive plane defining the error bar. Viewed from above (in figure 4.7(right)) the point of maximum likelihood and the error bars in the diffusivities can directly be extracted: The maximum likelihood is found at $\alpha = [2265, 0.75 \cdot 10^{-4}]$ (m^2/s). The 1/2-error bars lc arise as $a_{\text{hoc}} = (1560-3030)\text{m}^2/\text{s}$ and $a_v = (0.67-0.821) \cdot 10^{-4}\text{m}^2/\text{s}$. Compared to the subjective quantile represented by the Present Day Domain this represents a reduction of uncertainty in a_{hoc} of factor 3.1 (on logarithmic scale) and a reduction of factor 3.8 in a_v . This enormous learning effect is surely transferred into a reduction in spread of other climate relevant parameters (i.e. TCR, see section 4.4.1).

4.4 Transforming the learning effect to relevant climate parameters

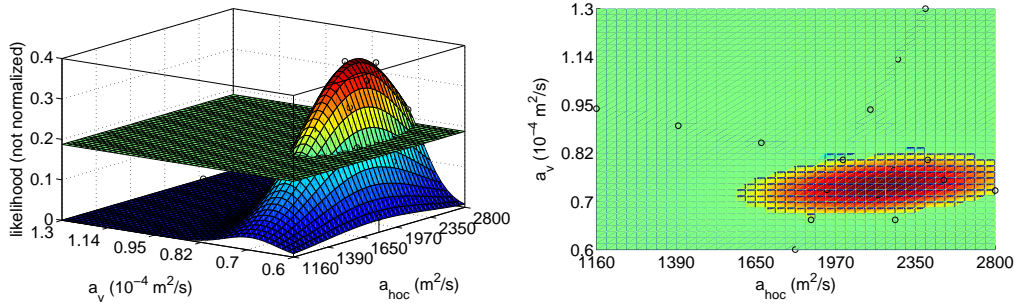


Figure 4.7: (left) Gaussian fit to the conditional likelihood $P(T|\alpha = [a_{\text{hoc}}, a_v])$, (right) the same viewed from above with the half-width of the fit

4.4 Transforming the learning effect to relevant climate parameters

To predict future climate evolution in a sensible way one has to know how sensitive Earth's climate system reacts to natural or anthropogen forcing such as emissions of greenhouse gases or aerosols. To get quantitative information about these sensitivities of the climate system, different measures of sensitivity were introduced. Two of them are Climate Sensitivity ($T_{2\times\text{CO}_2}$) and Transient Climate Response (TCR). Both quantities measure differences in global mean temperature. Climate Sensitivity is given as the difference in global mean temperature for a doubling of CO_2 from 280 to 560 ppm under the assumption of the system staying in (quasi)equilibrium. In the context of modeling this quantity is measured by starting a slowly rising (1% per year) CO_2 doubling scenario from an equilibrium state and afterwards letting the model run into equilibrium again for several thousand years. This approach takes into account the inertia of the climate system. This means, that only a small fraction of the overall reaction of the system to a distortion may be seen directly following the forcing but the (possibly) bigger part only emerges on centennial or millennial time scales.

4.4.1 Transient Climate Response (TCR)

For the prediction of the near future of the climate system, especially for the forthcoming century, mankind only faces the part of the climate response directly following the forcing signal. Thus the TCR measures the difference of global mean temperature in a 1% CO_2 doubling scenario from 280 ppm at present day climate to the point were 560 ppm of CO_2 concentration is reached (that is in year 71 of the simulation; see figure 4.15(left)).

The uncertainty in the knowledge of the TCR is represented by the uncertainty of the model's tuning parameters (e.g. the ocean diffusivities), meaning that one

4 Results & Interpretation

can tune the TCR by choosing the appropriate set of model parameters. When the uncertainty of the model parameters shrinks the domain of possible TCR values narrows. So by estimating the dependency $g(\alpha)$ of the TCR on the ocean diffusivities the learning effect of the 8.2 ka event on the ocean parameters can be transferred to the TCR (and other relevant parameters).

To estimate this dependency the TCR scenario was performed on a grid of 64 combinations of ocean diffusivity parameters, thereby covering the Ganopolski Domain. Figure 4.8 shows the results; in logarithmic representation of the ocean parameters the TCR shows a nearly linear dependency on $AHOC$ and A_{Kv} . The TCR decreases towards higher values of horizontal and vertical diffusivity; the dependence of the TCR on changes in horizontal diffusivity is smaller than on changes in vertical direction. A fit of the form

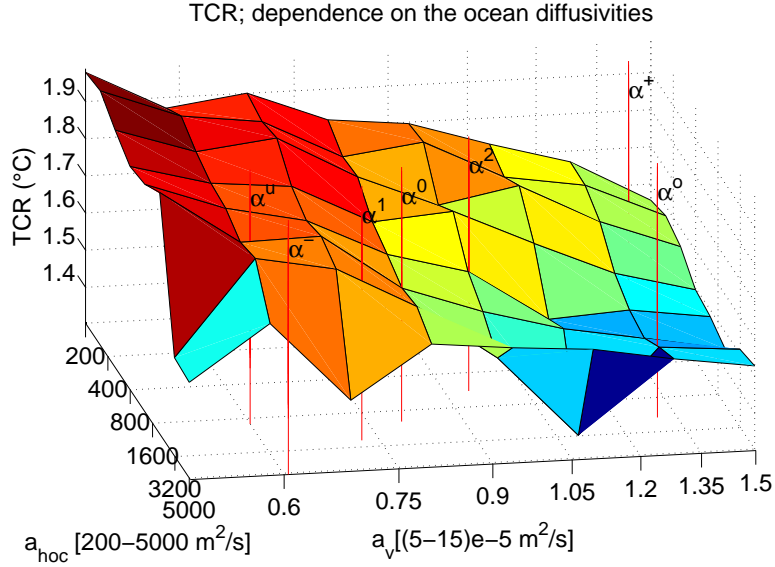


Figure 4.8: Transient Climate Response; dependence on the ocean diffusivities

$$TCR = a_1 + a_2 \cdot \log a_{hoc} + a_3 \cdot \log a_v \quad (4.1)$$

with $a_1 = -0.852 \pm 0.5$, $a_2 = -0.072 \pm 0.015$ and $a_3 = -0.3255 \pm 0.05$ [value, 95% quantile of fitting] is in good agreement with the measured dependency. Under this assumption of linearity in logarithmic space, the range of TCR within different domains in the two-dimensional space of ocean diffusivities can be directly calculated. Within the Ganopolski Domain CLIMBER-2.3 produces TCR values between the maximum value of $MAX_{GD} = (1.99 \pm 0.044)^\circ\text{C}$ and the minimum value of $MIN_{GD} = (1.401 \pm 0.043)^\circ\text{C}$. This leads to a quantile of $\Delta TCR_{GD} = (1.36 - 2.03)^\circ\text{C}$ within the Ganopolski Domain.

Within in the Present Day Domain the same approach leads to values of TCR

4.4 Transforming the learning effect to relevant climate parameters

between $\text{MAX}_{\text{SD}} = (1.82 \pm 0.03)^\circ\text{C}$ and $\text{MIN}_{\text{SD}} = (1.50 \pm 0.03)^\circ\text{C}$ and therefore to a quantile of $\Delta\text{TCR}_{\text{SD}} = (1.47 - 1.85)^\circ\text{C}$. This means a reduction of uncertainty in the quantile from the GD to the Present Day Domain (SD) by 43% (or a factor 2 of learning).

As experiments showed ca. 0.5°C of TCR uncertainty are not explainable by cs [Held et al. (2007)] and therefore have to originate from ocean uncertainty (compared SD quantile in figure 4.9). The Bayesian Learning in this study can address this remaining uncertainty and it constrains the parameter space even compared to the Present Day- or Schneider Domain and it delivers a likelihood function of conditioned relative frequencies within the boundaries of the prior domain. This additional information is transferred from $P(\alpha)$ to other outputs by involving the likelihood of all α_i with a certain TCR value according to equation (2.7). The resulting distribution of TCR values is shown in figure 4.9. The shape of the distribution is normal with mean $\text{TCR}_{\text{max,like}} = 1.70^\circ\text{C}$ as the likelihood over $\log(\alpha)$ has been estimated as multivariate Gaussian and the function $\text{TCR}(\log(\alpha))$ is fitted to be linear. Taking the interval in which the relative frequency decreases to $1/e$ of its maximum the error bar (lc) reads $\Delta\text{TCR}_{\text{new}} = (1.65-1.75)^\circ\text{C}$. This error bar enables three different interpretations: Firstly the $1/e$ error bar can be interpreted as ratio of likelihood without need of any prior distribution, thereby loosing a probabilistic measure but gaining objectivity. Secondly, as the prior distribution on Ganopolski- and Present Day-Domain is taken to be uniform on logarithmic scale the error bar lc also can be interpreted as probability ratio. Finally the Gaussian shape of the TCR histogram allows to interpret lc as posterior quantile. The fitted Gaussian function encloses a probability between 65% (1σ) and 95% (2σ) within the part above the $1/e$ -level. This level corresponds to a variance of $\sqrt{2}\sigma$. Therefore lc represents a reduction of uncertainty in TCR of factor 3.8 compared to the Present Day Domain.

4.4.2 Climate Sensitivity ($\text{T}_{2\times\text{CO}_2}$)

As the Climate Sensitivity (or cs) co-determines the temperature response to anthropogenic greenhouse gas forcing and therefore is needed to estimate α_{res} (see section 4.4.3) the learning effect on the ocean diffusivities is also transferred to $\Delta\text{T}_{2\times\text{CO}_2}$ by applying the same method as in section 4.8. The dependence of cs on the diffusivities $\text{T}_{2\times\text{CO}_2} = g(\alpha)$ is estimated from the CO_2 doubling scenario described at the head of this section as difference in equilibrium temperatures $\text{T}_{2\times\text{CO}_2}|_{\alpha} = T(560\text{ppm})|_{\alpha} - T(280\text{ppm})|_{\alpha}$. The result is shown in figure 4.10. While cs is nearly constant for small values of a_{hoc} and a_v it shows a characteristic broad maximum for certain log linear combinations of vertical and horizontal diffusivity with a fast decreasing tail towards the upper border of the Ganopolski Domain. This result is surprising as the Climate Sensitivity being a non transient entity should not depend on ocean heat capacity. The dependency of cs on ocean diffusivity is assumed to originate from the ice-albedo feedback

4 Results & Interpretation

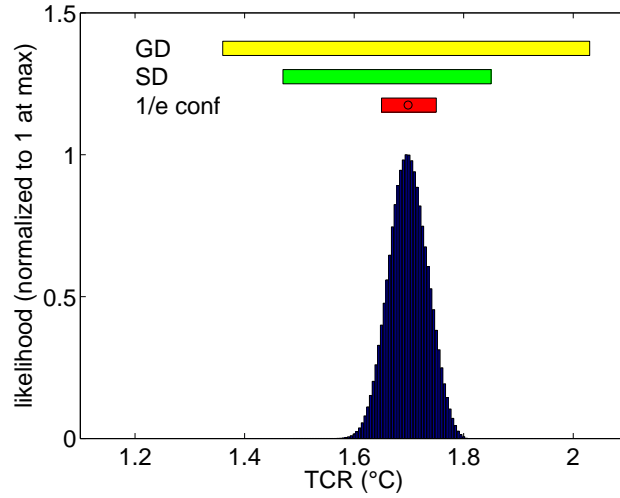


Figure 4.9: Likelihood of Transient Climate Response; normalized to 1 at max; the quantiles of Ganopolski Domain (GD), Present Day Domain (SD) and the 1/e error bar (lc) of the likelihood are shown.

and the dependence of sea ice on the ocean diffusivities. As the functional form

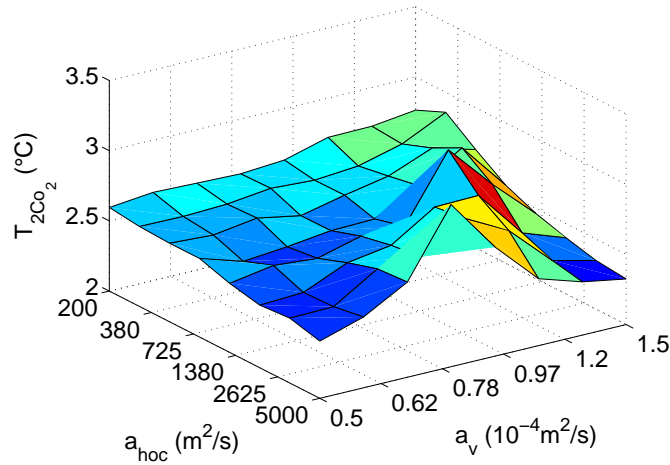


Figure 4.10: Climate sensitivity; dependence on the ocean diffusivities (over GD)

of $\Delta T_{2 \times CO_2} = g(\alpha)$ is not well suited to be fitted by a Gaussian or log linear function, the data are interpolated on a grid covering the Present Day Domain. This study is not able to be informative about a reduction in uncertainty of cs because the most influential parameters on cs (like cloud parameters) were taken as constants. But the estimated functional dependence of cs on the ocean diffusivities

4.4 Transforming the learning effect to relevant climate parameters

is used to transfer the learning effect to the temperature response parameter α_{res} in the following section.

4.4.3 Climate response parameter α_{res}

To relate the Bayesian Learning to a climate system parameter that is a key for qualitative aspects of climate projections the reduction of uncertainty is transferred to a parameter in a climate model used by Kriegler and Bruckner (2005) to calculate emission pathways and the influence of normative constraints on emission utilizing the *tolerable window approach* (TWA) [Tóth et al. (1997), Bruckner et al. (1999), Petschel-Held et al. (1999)]. In this simple model by [Petschel-Held et al. (1999)] the response of global averaged climate to anthropogenic forcing is described by the following equations:

$$\dot{F} = E \quad (4.2)$$

$$\dot{C} = \beta E + BF - \sigma C \quad (4.3)$$

$$\dot{T} = \mu \ln c - \alpha T \quad \text{with} \quad c = \frac{C + C_{pi}}{C_{pi}} \quad (4.4)$$

This model simulates the evolution of the global mean temperature anomaly T relative to the preindustrial level responding to anthropogenic emission of CO_2 (E) that sum up to the cumulative emission F and contribute to the atmospheric CO_2 concentration anomaly C relative to preindustrial level. The temperature equation (4.4) directly leads to the Climate Sensitivity $T_{2 \times \text{CO}_2}$ by considering the case $\dot{T} = 0$, $c = 2$ (doubling of CO_2):

$$T_{2 \times \text{CO}_2} = \frac{\mu}{\alpha} \ln 2 \quad (4.5)$$

Taking different assumptions discussed by Kriegler and Bruckner (2005) the parameters μ and α of equation (4.4) can be linked to three physical quantities: the effective ocean heat capacity c_{oc} , the radiative forcing for a doubling of preindustrial CO_2 level $Q_{2\text{CO}_2}$ and Climate Sensitivity $T_{2 \times \text{CO}_2}$:

$$\mu = \frac{Q_{2\text{CO}_2}}{c_{oc} \cdot \ln 2}, \quad \alpha = \frac{Q_{2\text{CO}_2}}{c_{oc} \cdot T_{2 \times \text{CO}_2}} \quad (4.6)$$

As the integral form of equation (4.4) shows:

$$T(t) = e^{-\alpha(t-t_0)} \int_{t_0}^t \mu \ln c(t') e^{\alpha t'} dt' \quad (4.7)$$

4 Results & Interpretation

the parameter α_{res} represents an inverse time scale for the decay of an anthropogenic perturbation of global mean temperature. The transfer from TCR and CS (Climate Sensitivity) to α_{res} can be achieved by solving:

$$\frac{T_{2\times\text{CO}_2}}{\ln 2} \cdot \frac{h}{\alpha_{\text{res}}} - \text{TCR} = 0 ,$$

with

$$h = \gamma(-1 + \exp(-\alpha_{\text{res}}t) + \alpha_{\text{res}}t) + \alpha_{\text{res}} \log(c0)(1 - \exp(-\alpha_{\text{res}}t)) ;$$

$\gamma = \log(1.01)$, thereby using equation (4.5) and (4.7) for the case $c(t) = 2$ and assuming exponential increase of CO_2 . The linkage between the diffusivities and the temperature response parameter α_{res} is shown in figure 4.11. As in the case of TCR and CS the transferred learning effect due to the assimilation of the 8.2 ka event is considerably high compared to the knowledge gained from Ganopolski- and Schneider Domain only (see figure 4.12). The learning effect on the parameter μ representing the pure reaction of the ocean without interference of cs is shown in figure 4.13. The corresponding timescale $\tau = 1/\alpha_{\text{res}}$ is constrained by Bayesian Learning to (22-30) yrs compared to (17-48) yrs on GD and (21-41) yrs on SD (see figure 4.14). This timescale τ allows to estimate the climate response to short scale forcing such as the scenario of China rapidly reducing the aerosol emission within only several years thereby producing a Heaviside-like additional global radiative forcing. An example of a corresponding forcing and response is shown in figure 4.15. This aerosol extraction scenario is equivalent by order of magnitude to a rapid increase of global mean temperature for a jump in CO_2 concentration of about 100 ppm CO_2 in 2020. This amount of CO_2 is added to a standard TCR scenario under the assumption that the extraction of China's aerosols corresponds to a temperature jump of 1°C which is translated to a CO_2 equivalent of 100 ppm. The rapid increase of GMT slows down exponentially as projected by the small climate model (equation (4.4)). Thus the global temperature response of CLIMBER-2.3 to the aerosol extraction scenario can be emulated by the small model with good agreement (not quantified here).

The small climate model represented by equations (4.2)-(4.4) is used to calculate emission pathways subject to normative constraints on global temperature rise. In this context the temperature response parameter represents the inertia of the climate system when reacting on changes in global emissions. If now industry commits to a climate regime with the aim of not passing a temperature threshold the question arises when best to shift capacities to carbon free technologies. On the other hand a shorter climate reaction time scale increases the impact of climate policies as measures against global warming will quickly show an impact.

4.4 Transforming the learning effect to relevant climate parameters

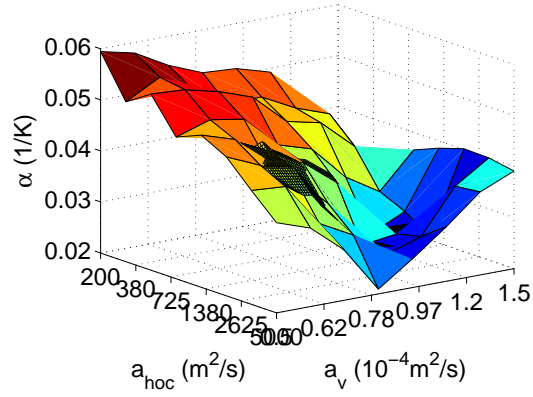


Figure 4.11: Temperature response parameter α_{res} over the diffusivity space covering the GD

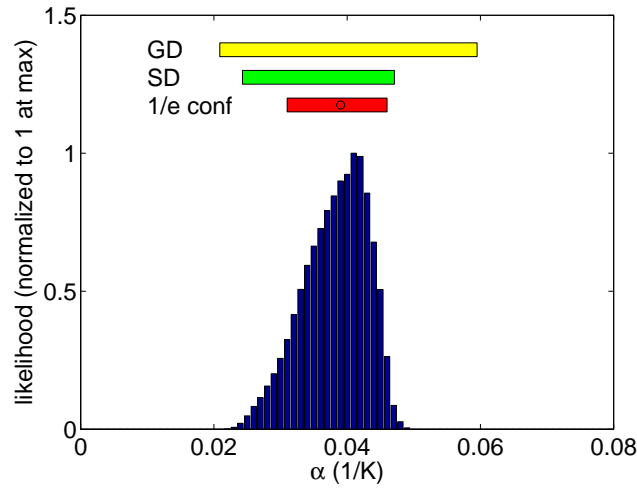


Figure 4.12: Likelihood of temperature response parameter α_{res} ; normalized to 1 at max; the quantiles of Ganopolski Domain (GD), Schneider Domain (SD) and the 1/e bar (of a Gaussian fit) of the likelihood are shown

4 Results & Interpretation

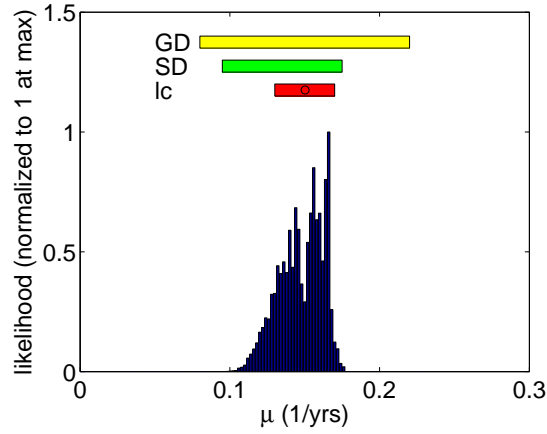


Figure 4.13: Likelihood of ocean response parameter μ ; normalized to 1 at max; the quantiles of Ganopolski Domain (GD), Present Day- or Schneider Domain (SD) and the 1/e error bar of the likelihood are shown

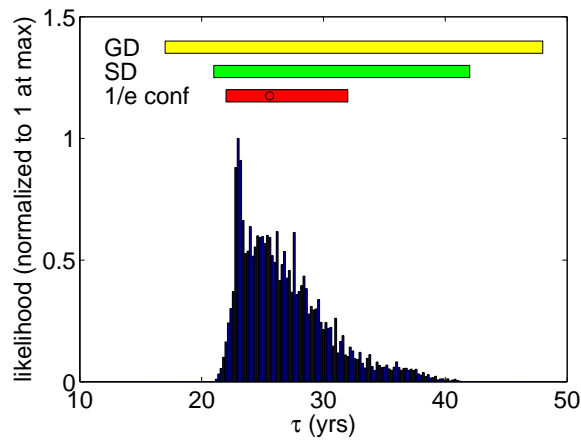


Figure 4.14: Likelihood of temperature response time scale $\tau = 1/\alpha_{\text{res}}$; normalized to 1 at max; the quantiles of Ganopolski Domain (GD), Present Day Domain (SD) and the 1/e error bar of the likelihood are shown

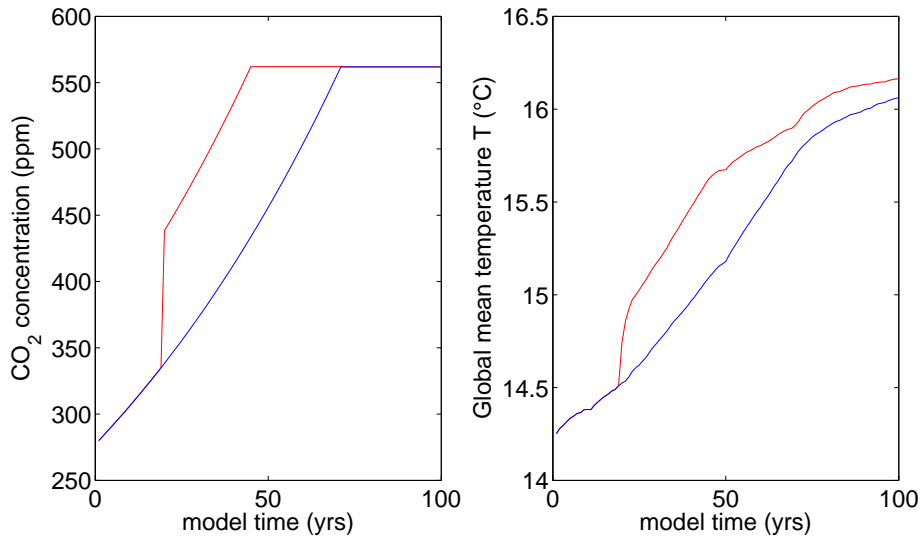


Figure 4.15: (left) CO₂ forcing for the TCR (blue) and a sulfate extraction (red) scenario and (right) the corresponding global mean surface temperature

4.5 Summary

With the setup described in section 3.1.1 CLIMBER-2.3n reproduced a cold event comparable to the findings of Bauer et al. (2004). As the model's performance strongly depended on the realization of freshwater noise η the run was repeated 150-300 times per parameter setting with different seeds for the noise generator. The resulting histograms of durations of the cold event were produced. This systematic approach of including the influence of freshwater noise revealed the existence of at least two different modes of cold event duration: One centered around 80 years and a second mode with a center strongly dependent on the duration of the additional baseline flux in the experiment. One possible explanation for the existence of two modes bases on the different states of the overturning circulation in the northern Atlantic explored by Bauer et al. (2004). The short mode may originate from the recovery from INT to ON mode whereas the long mode originates from a recovery from the OFF mode. This explanation was ruled out by comparing the corresponding overturning stream functions which showed no characteristic differences between runs with short and such with longer cold event duration.

The first mode represents a timescale (about 10^2 yrs) that corresponds to the advective time scale of the whole Atlantic and therefore points to an at least hemispherical range of the 8.2 ka event. As the first mode hardly depends on the experiment related parameters, CLIMBER-2.3 is not able to reproduce the

4 Results & Interpretation

right duration of the 8.2 ka event (with considerably high likelihood) within a one-pulse scenario without additional baseline fluxes. This conclusion indicates a crucial role of future investigations of more complex freshwater forcing scenarios and the corresponding data.

Although the additional experiment-related parameters showed strong influence on the likelihood of the diffusivities they were kept constant in the following first iteration to calculate the conditional likelihood of the ocean diffusivity parameters in two dimensions. Taking the 1/2-level as error bar the resulting likelihood shows a reduction of uncertainty by factor 3 in the horizontal and factor 3.8 in vertical ocean diffusivity compared to prior knowledge.

To use the learning effect in discussions of climate change and mitigation it has been transferred from CLIMBER-2.3 ocean diffusivity parameters to the Transient Climate Response (TCR). The range of values of TCR, which could not be explained by uncertainty in Climate Sensitivity, was reduced by 0.3°C compared to the prior knowledge. The general range of values for the climate characteristics is constrained by taking only standard values for all other parameters in CLIMBER-2.3. A throughout analysis of their influence would lead to a range of TCR and $T_{2\times CO_2}$ comparable to GCM performance (see von Deimling et al. (2006)).

Finally to estimate the impact of the learning effect on mitigation policies for avoiding dangerous climate change it has been transferred to the temperature response parameter α_{res} . This parameter represents the time scale of the climate's linearized reaction to abrupt anthropogenic distortions of global mean temperature by emission of CO₂. The range of this time scale has been reduced from (21-41) years to (22-32) years by the Bayesian Learning implementation.

5 Discussion

A scheme has been presented how to Bayesian learn from paleo-data on uncertain climate parameters. Employing CLIMBER-2.3 this method was implemented to constrain model parameters representing horizontal and vertical ocean diffusivities by assimilating Greenland ice core data from the 8.2 ka event. Within affordable costs of computation the likelihood of the diffusivity parameters was estimated from ensemble runs of the noisy version of CLIMBER-2.3. The method led to considerable reductions of uncertainty in the ocean diffusivities (factor 3 vs. prior knowledge) and in climate-relevant parameters like TCR and climate response parameter α_{res} . So far the method of Bayesian Learning has proven highly valuable.

Nevertheless different imperfections corrupt the success of the implementation. The limited availability of computational power constrains the number of ensemble runs to be performed. This constraint was faced by reducing the dimension of the problem in several places: Firstly the basis of comparison between model and data was chosen as one-dimensional output; the duration of the cold event. A more sophisticated comparison of time series of data fields would preserve more information of the 8.2 ka event at the cost of a tremendous need for computational power. The strength of the approach of directly estimating the likelihood from ensemble runs is that no specific functional form has to be assumed a priori; again leading to higher computational effort. Secondly the number of parameters to learn on had to be constrained. In a first iteration the method was demonstrated by choosing only two-dimensional learning on the diffusivities with all other parameters taken as known constants.

There exist two different ways to overcome this imperfection: Without using more data, the likelihood can be expanded to higher dimensions, which only takes more computation again (and an intelligent sampling strategy) or the other parameters can be constrained by including additional sources of information such as other data or a consensus of expert knowledge. It is obvious that when adding more uncertain parameters the uncertainty in each single parameter rises. So for each implementation of Bayesian Learning a balance between complexity in model data comparison and complexity in learning space must be found.

The use of additional input is explored in section 5.1 where autocorrelation of salinity fields is used to link the uncertain diffusivity to other parameters. Those links provide the possibility to freely choose the parameter that is most suitable to be measured and the one to learn on indirectly through the Bayesian method.

5 Discussion

In section 5.2 the expansion of the problem to three dimensions by taking into account different volumes of baseline flux is described. This additional uncertainty strongly reduces the learning effect on the diffusivities thereby revealing the limits of information to gain by this experimental setup.

Overcoming these imperfections by including more uncertain parameters and including more data aims at the comparability of the results. One has to keep in mind that the employed model and data themselves set limits on how close the result can get to reality. When using the CLIMBER-2.3 derived temperature response timescale $\tau = 22\text{-}32$ yrs one has to consider that GCMs show a strong influence of nonlinear effects on decadal scale. So the predictive strength of a linear response parameter is weakened.

Another aim of this study, besides proving the value of Bayesian Learning, is to show in principle how to close the circle to an integrated assessment by transferring the learning effect to an economic context. The reduction of uncertainty has been transferred to other parameters (e.g. TCR, CS, α_{res}) which are central in research concerning climate change. The impact of the reduction of uncertainty in α_{res} on mitigation policies is qualitatively discussed in section 5.3.

5.1 Using additional sources of information - Autocorrelation of salinity- and temperature field data

Held and Kleinen (2004) presented a method to estimate the proximity of a dynamic system like a climate subsystem to non linear thresholds, e.g. a shutdown of the thermohaline circulation. The so called Degenerate Fingerprinting rests on constructing a control parameter κ that is highly informative on the proximity to the shutdown. The parameter κ is motivated by investigating a theoretical situation of a bifurcation. This requires several assumptions: The systems quasi-stationary dynamic is simplified as an equilibrium of a deterministic dynamic that is perturbed by weather generated noise; the response to noise is approximated by linear modes (small noise limit). Under these assumptions Held and Kleinen (2004) identified a “critical mode” defined by the smallest decay rate κ that vanishes at the bifurcation. In the small noise limit this mode is represented by the leading EOF of the field under consideration. So Held and Kleinen (2004) used the projection of the salinity field onto the first EOF obtained from time series with standard diffusivities and the freshwater forcing closest to the bifurcation as proxy for the critical mode dynamics. Under the assumption of vicinity to the bifurcation the temporal evolution is simplified to a one-dimensional autoregressive process (AR(1)-process) $y_{n+1} = cy_n + \sigma\eta_n$, with $c = \exp(-\kappa\Delta t)$ and η_n Gaussian white noise. By definition the propagator c takes values in $[0, 1]$ with 1 at the bifurcation (as the critical decay rate κ vanishes). The method requires

5.1 Using additional sources of information - Autocorrelation of salinity- and temperature field data

a separation of time scales between the critical mode (with decay rate κ) and the other modes (with decay rate κ_i). Therefore the time step Δt of the AR(1) process has to fulfill the requirement:

$$1/\kappa \ll \Delta t \ll 1/\kappa_i . \quad (5.1)$$

In this study the method is used to link the ocean diffusivities α , the freshwater forcing μ and the distance to the bifurcations represented by the propagator c . For different values of α and μ (using factorial design) noisy equilibrium runs of CLIMBER-2.3 are performed. Each time serie of the salinity field covers 10,000 years with time step $\Delta t = 50$ yrs (which has shown consistent with (5.1) in the equivalent setting; see Held and Kleinen (2004)). The first 5,000 years are removed as start up phase for CLIMBER-2.3 to reach near equilibrium. As the AR(1) process only works on stationary time series distorted by white noise, a quadratic trend is removed from the Atlantic salinity field. Afterwards it is projected onto its first principal component (shown in figure 5.1). The boxes representing the surface layer at $(50-70)^\circ$ N are left out because of their direct dependence on the freshwater forcing. The resulting time series are fitted with a AR(1)-process by estimating the propagator c from autocorrelation with step-width one (lag-1 operator). Figure 5.1 shows the propagator c over the Ganopolski Domain in diffusivity space for different values of freshwater forcing (standard forcing - 0.1 Sv (lower), standard forcing (middle) and standard forcing + 0.1Sv (upper)). Qualitatively it shows the dependence of the proximity to a bifurcation on the freshwater forcing: The propagator increases towards higher levels of freshwater forcing with constant diffusivities; for constant freshwater forcing the propagator rises mainly with increasing horizontal diffusivity.

This linkage opens different valuable possibilities for constraints on uncertainties: Following the assumptions of section 4.3.1 namely that the freshwater forcing (in terms of the 8.2 ka event the known background flux) is constant at the known standard level the new linkage can be used to further reduce the uncertainty of the diffusivities. Alternatively one can use the link to transfer the learning effect on the diffusivities to a learning effect on the propagator and thus constraining the proximity to a THC breakdown. The second is shown in figure 5.1. The learning effect is transferred to the propagator of the AR(1) process following the procedure described in section 4.4. So given the strength of freshwater runoff (standard value) and the posterior distribution of diffusivities the propagator c is constrained to $c = 0.63-0.67 [0.65]$ in $1/e$ -likelihood error bar compared to $c_{GD} = 0.4877-0.8518$ for the Ganopolski Domain and $c_{SD} = 0.5425-0.7165$ for the Present Day Domain. This represents a reduction of uncertainty of factor 5 vs. SD and of factor 10 vs. GD.

5 Discussion

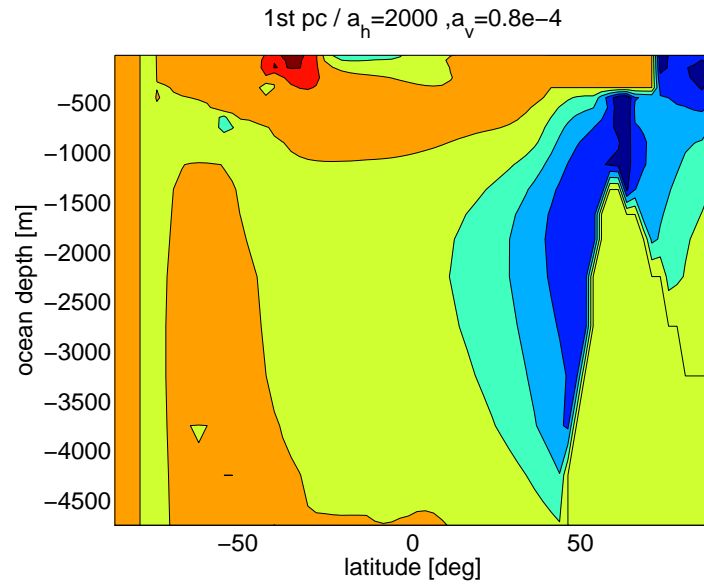


Figure 5.1: First principal component (1st pc) of Atlantic salinity field for standard diffusivities

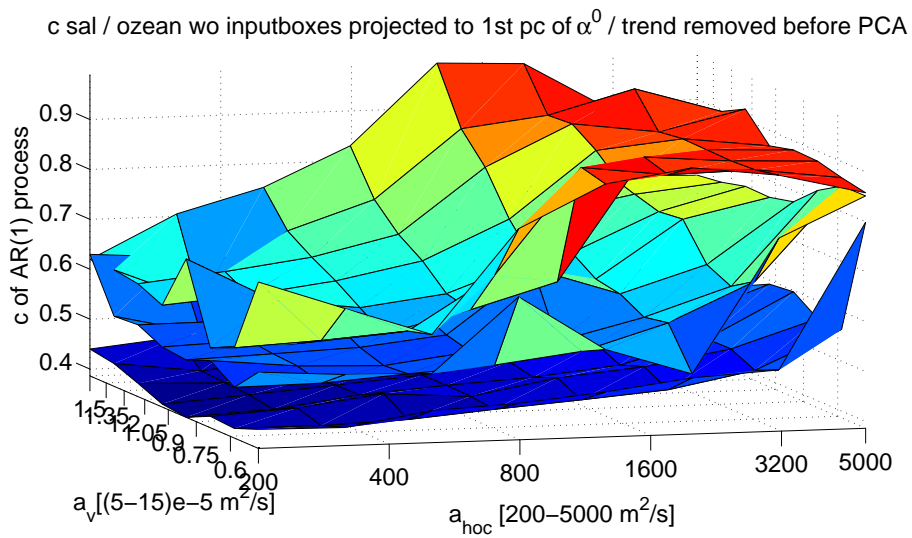


Figure 5.2: Atlantic AR(1) propagator c over the two-dimensional domain of ocean diffusivities for different values of freshwater runoff into the northern Atlantic (bottom = standard-0.1 Sv, middle = standard, upper = standard+0.1 Sv)

5.2 Including additional parameters; strength FW of baseline flux

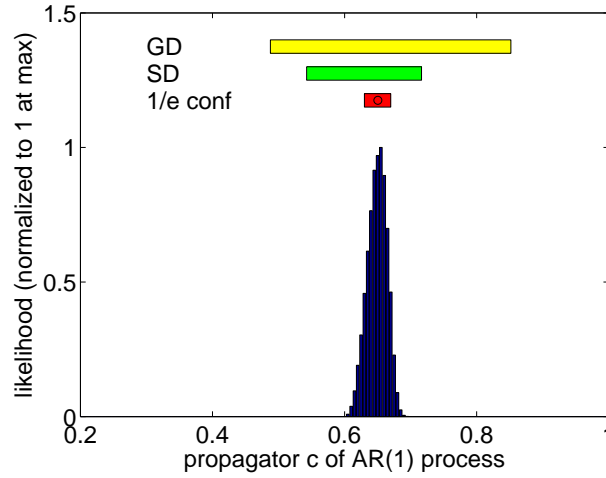


Figure 5.3: relative frequency distribution of the Atlantic AR(1) propagator c for standard value of freshwater runoff into the northern Atlantic after the Bayesian Learning on the diffusivities

5.2 Including additional parameters; strength FW of baseline flux

So far the learning effect presented in this study was achieved by neglecting the uncertainty of all parameters but the ocean diffusivities. Although this approach proves the possibility to constrain uncertain model parameters by ‘assimilating’ paleo-data containing the 8.2 ka event the comparability of the outcome to other studies can only be achieved by including other uncertain parameters. To get a robust result inside the stylized CLIMBER world one has to include the uncertainty of all experiment related parameters at least. These are the amplitude of freshwater noise and strength and duration of the additional freshwater baseline. Including the uncertainty of additional parameters drastically enlarges the complexity of the problem to estimate the likelihood. Within the context of the 8.2 ka event the necessity of directly estimating the unknown likelihood from ensemble simulations places a constraint to the manageable complexity in learning space. As a first step to improve the soundness of the learning effect the strength FW of the baseline flux employed in the 8.2 ka simulations is included as an uncertain parameter. The influence of the uncertainty of FW on the now three-dimensional likelihood has been investigated by a nearly factorial sampling design. As the 2D likelihood is known to be well represented by a Gaussian fit in logarithmic diffusivity space the sampling follows the assumption that the influence of FW can also be modeled as Gaussian. For eight points in diffusivity space the 8.2 ka simulations have been repeated with altered values of FW (0.015 Sv and 0.045

5 Discussion

Sv against 0.03 Sv in standard). The multi-dimensional Gaussian fitting routine has been extended to three dimensions.

The resulting fit of the likelihood projected onto diffusivity space is shown for $FW = 0.03$ Sv in figure 5.2[left]. The half-width of the likelihood taken as error bar defines the posterior quantile shown in figure 5.2[right]. The influence of FW on the error quantile in two-dimensional diffusivity space is demonstrated in figure 5.5 that shows the half-width error quantile for three different values of FW . The comparison of the error quantile in figure 5.2[right] to the same setting in figure 4.7[right] shows a stronger spread especially in a_{hoc} for the three-dimensional application of the fitting routine.

This leads to several possible conclusions: The number of measurements might have been insufficient to constrain the fitting in a sensible way (the spread is overestimated in figure 5.2). Alternatively the assumption of Gaussian shape likelihood in FW may be misleading. In both cases a more sophisticated sampling scheme would be needed to investigate the shape of the three-dimensional likelihood. If the likelihood had at least a global maximum an optimization approach could be of use (Seidel approach). Although the fitting routine overestimated the range in diffusivity space and thereby wiped out the learning effect in a_{hoc} the range in a_v does not increase by large. By changing FW within [0.015-0.045] Sv the range in the vertical ocean diffusivity parameter is increased to $[0.62 - 0.87] \cdot 10^{-4} \text{m}^2/\text{s}$ compared to $[0.68-0.82] \cdot 10^{-4} \text{m}^2/\text{s}$ in figure 4.7[right]. The uncertainty of FW hardly weakens the learning effect on vertical ocean diffusivity but diminishes the learning effect on horizontal diffusivity. This means that additional information is needed to regain the whole learning effect. This can be done either by independently constrain the baseline flux from other paleo-data or to enlarge the base of model-data comparison.

5.3 Impact of the learning effect on climate policy

Now one would like to ask whether there are already some qualitative conclusions one could draw for climate policy, under the scenario that the results obtained so far could be confirmed by more complex models and a more comprehensive statistical analysis. As a main result of the present study it can be obtained that uncertainty on climate response time scale could be reduced to the lower half of the interval in time scale. This would have the following implications:

Previous work on constraining climate sensitivity from the signal of anthropogenic warming within the 20th century faced - among other difficulties - the problem to disentangle the joint effect of Climate Sensitivity and response time scale on the warming signal: The warming may result from low Climate Sensitivity combined with fast response, or large sensitivity combined with slow response. If

5.3 Impact of the learning effect on climate policy

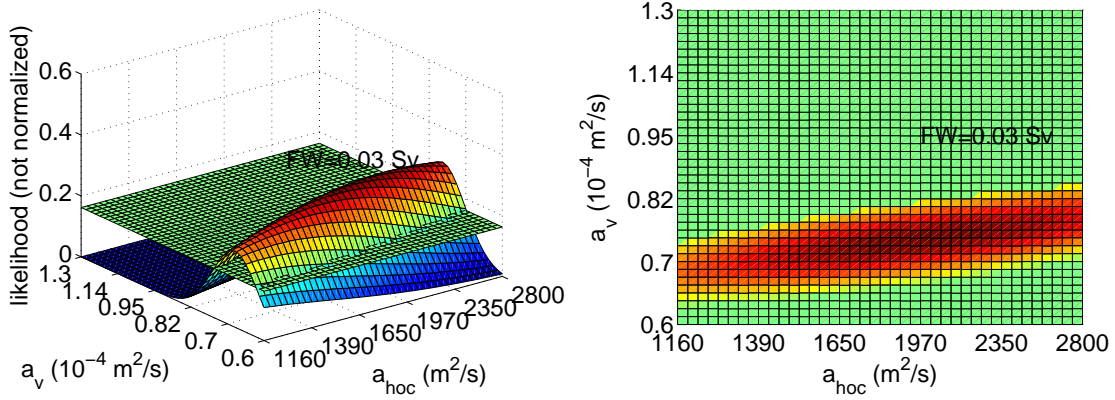


Figure 5.4: (left) Gaussian fit to the conditional likelihood $P(T|\alpha = [a_{\text{hoc}}, a_v, \text{FW} = 0.03\text{Sv}])$, (right) the same viewed from above with the half-width of the fit

one could exclude the slow response end, that would point towards the lower end of Climate Sensitivity. This finding would be in-tune with, hence would further confirm, results from von Deimling et al. (2006), who also excluded high-end Climate Sensitivity well beyond 5°C . In terms of a hedging strategy this implied that society would not have to hedge against very extreme values of sensitivity, which implied a net gain in global welfare production (GWP): As Held et al. (2007) could show, GWP costs for mitigation scale with Climate Sensitivity as about 0.5% per $^\circ\text{C}$. Given a current GWP of $0.4 \cdot 10^{14}$ US \$ per year, this would attribute a severe economic value to that Bayesian Learning. Furthermore, within a Bayesian framework, any information stemming from statistically independent data sources, tends to sharpen the overall posterior distributions. Hence, when combining the results from von Deimling et al. (2006) with the present work, a further narrowing of the error bars on Climate Sensitivity can be expected. Finally, lower values of Climate Sensitivity imply a lower total carbon stock that could still be emitted within this century, given a particular global temperature cap. For potential anthropogenic interventions that are much faster than CO_2 concentration increase, it can be concluded that climate response is more on the fast side of what has been proposed so far, hence the time scale effect would dominate that of lower Climate Sensitivity for abrupt changes in forcing. This is of relevance for desulphurization policy within the fossil fuel sector, as sulfate aerosols currently impose a significant global cooling effect. In case countries like China and India decided for an abrupt SO_2 mitigation policy this could have severe consequences for the likelihood of observing global temperature caps. This would enhance the pressure for earlier CO_2 emission mitigation while the overall stock of carbon allowed to be emitted stays lower (see above). Projecting SO_2

5 Discussion

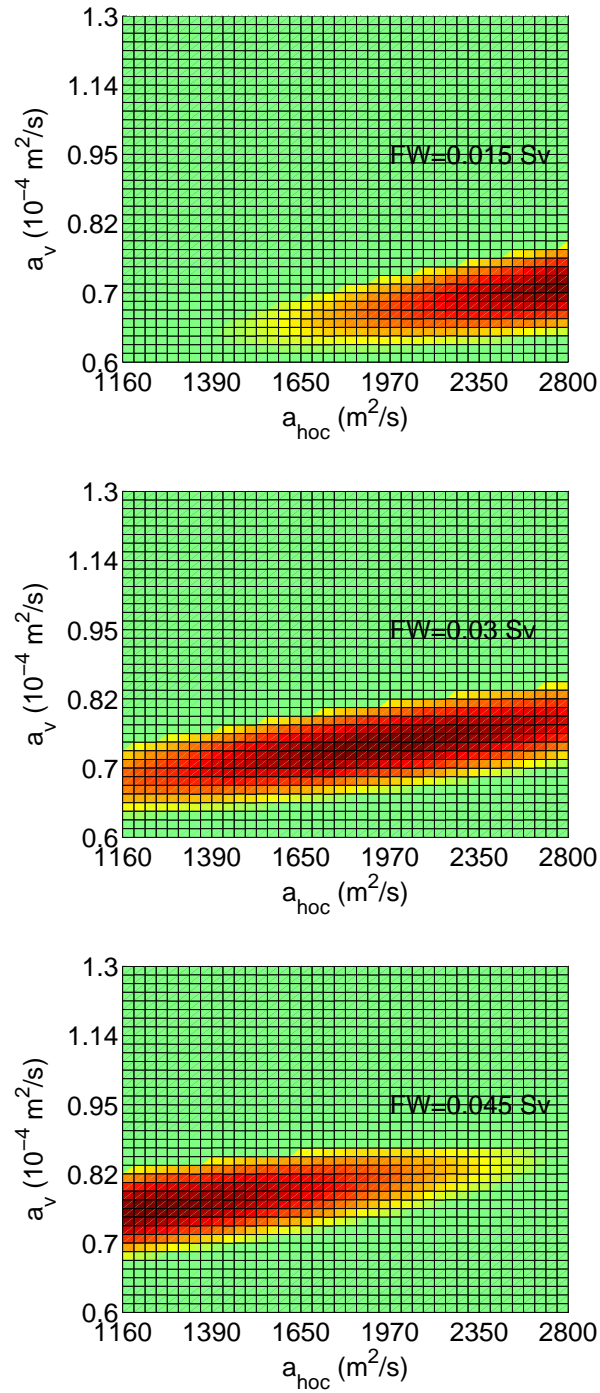


Figure 5.5: 1/2 error bar of a Gaussian fit to the conditional likelihood $P(T|\alpha = [a_{\text{hoc}}, a_v, \text{FW}])$ for different values of FW (upper: FW = 0.015Sv, middle: FW = 0.03Sv, lower: FW = 0.045Sv)

5.3 Impact of the learning effect on climate policy

emissions until 2020, this could make up a difference in global mean temperature on the order of 1°C (E. Bauer, H. Held, private comm.).

5 *Discussion*

6 Summary & Outlook

In this study a Bayesian Learning scheme has been successfully implemented by employing CLIMBER-2.3 to constrain ocean diffusivity parameters from Greenland paleo-data containing the 8.2 ka event. Ensemble simulations of the 8.2 ka cold event in CLIMBER-2.3 revealed a time scale of cooling that points towards an at least hemispherical range of the event. The inability of CLIMBER-2.3 to reproduce the right duration of cooling within a one-pulse scenario emphasizes the importance of including additional continental runoff around the 8.2 ka event.

The resulting learning effect on the diffusivity parameters showed a reduction in uncertainty of factor 3 compared with prior knowledge. This learning effect has been transferred to other climate-relevant parameters, such as TCR, α_{res} and propagator c , to reduce uncertainty of various aspects of future climate evolution such as proximity to bifurcations or time scale and amplitude of changes in temperature due to changes in greenhouse gas emissions. By linking the parameters from natural systems to model parameters in socio-economic context the impact of the Bayesian Learning on climate policies and decision making processes has been discussed.

As discussed in section 5.3 the transformation of the learning effect on model parameters to factors which are important in socio-economic modeling revealed a net benefit in terms of GWP. So in future studies the importance of investigation in different parameters can be compared. In the same way different data sets can be compared according to their potential to reduce uncertainty in important socio-economic factors. In this way the Bayesian approach not only improves the confidence in model projections but provide a rational measure of importance for different possible investigations.

The limited availability of computational power rises constraints on the dimension of model-data comparison and the dimension of parameter space to be investigated by Bayesian Learning. Due to this imperfections all results presented here prove valid in the stylized CLIMBER-2.3 world only. Therefore this study can only be seen as a preliminary investigation of the feasibility and value of the Bayesian assimilation scheme. A more sophisticated treatment of the subject by using more complex models (paleo-GCMs) and data (e.g. SST reconstructions for equatorial Atlantic, reconstructions of precipitation in monsoon regions) has to follow.

6 *Summary & Outlook*

Zusammenfassung in deutscher Sprache

„Unsere Welt ist unsicher“ [Howson and Urbach (1991)]. Dies gilt insbesondere, wenn man komplexe Systeme wie das Klimasystem der Erde betrachtet. Diese Unsicherheit begrenzt unser Wissen über die Zukunft unabhängig davon, ob sie unserer eigenen Unvollkommenheit wie mangelndem Systemverständnis oder begrenzter Rechenkapazität oder der starken Nichtlinearität des Systems oder elementarem Zufall entspringt. Deshalb ruht jeder Versuch einer Prognose über die zukünftige Entwicklung des Klimasystems auf einer Vermutung, die in unserem aktuellen Wissen über das System gründet. Die Modellierung des Klimas ist eine formalisierte Version der Vermutung, die das verfügbare Wissen über Systemzusammenhänge konsistent zusammenführt. Ein Teil unserer Unsicherheit ist in den Modellen in Form frei einstellbarer Parameter repräsentiert. Entsprechend zeigen die Modelle eine Vielzahl verschiedener möglicher Szenarien zukünftiger Entwicklung. Es bleibt das prinzipielle Problem, zwischen wohlbegründeten Vermutungen und reinen Spekulationen zu unterscheiden. Ein möglicher Ansatz besteht darin, den Prognosen derjenigen Modelle zu vertrauen, welche möglichst viele Phänomene und Charakteristika des heutigen und vergangenen Klimas reproduzieren können. Diese Gewichtung von Parametersätzen für Modelle anhand von Paläodaten wird durch den Bayesschen Formalismus beschrieben.

Bisherige Studien über Bayessches Lernen mit dem Klimamodell CLIMBER-2.3 haben sich zentral mit der Einschränkung der Unsicherheit der Klimasensitivität befasst, also mit *Gleichgewichtseigenschaften* des Klimasystems. Der zentrale Ansatz dieser Arbeit besteht darin, für das Bayessche Lernen einen anderen Pool von Paläodaten zu nutzen, von denen eine starke Korrelation zur globalen effektiven Wärmekapazität des Ozeans erwartet wird. Diese Größe hat starken Einfluss auf die Bestimmung der *Zeitskala* der Reaktion des Klimasystems auf anthropogene Treibhausgasemissionen und damit (zusammen mit der Klimasensitivität) auf die Festlegung „optimaler“ Klimapolitik. Eine frühere Arbeit von Bauer et al. (2004) hat gezeigt, dass CLIMBER-2.3 in der Lage ist, das 8.2 ka Ereignis nachzubilden. Diese Arbeit ruht auf der Annahme, dass das 8.2 ka Ereignis stark von den Ozeandiffusivitäten bestimmt wird, welche ihrerseits die Wärmekapazität maßgeblich mitbestimmen.

Diese Arbeit setzt sich als Ziel, mittels Bayesschen Lernens einen dynamisch konsistenten Bogen vom 8.2 ka Ereignis bis zur Zeitskala der Reaktion des Klimasystems auf Treibhausgasemissionen zu spannen. Dazu wird ein Schema zur

6 Summary & Outlook

Implementierung des Bayesschen Lernens aus Paläodaten präsentiert. Der Fokus liegt dabei auf Isotopendaten aus den grönländischen Eisbohrkernen, die das prominente 8.2 ka Kaltereignis beinhalten. Da dieses Ereignis in extremer Weise aus dem sonst stabilen Klima des frühen Holozäns heraussticht, ist von dem Modell-Daten Vergleich eine starke Einschränkung der Unsicherheiten der Ozeanparameter zu erwarten. Da das 8.2 ka Ereignis in CLIMBER-2.3 stark nichtlinear von den unsicheren Ozeandiffusivitäten abhängt, kann die Likelihood der Diffusivitäten nicht wie allgemein üblich a priori als gaußförmig angenommen werden. Dieser Schwierigkeit wird durch Anwendung einer verrauschten Version (CLIMBER-2.3n) des Klimamodells begegnet, mit dem die Likelihood der Ozeandiffusivitäten aus Ensembleexperimenten numerisch aufgebaut wird.

Als Ergebnis dieser Studie erbrachte das Bayessche Lernen eine Einschränkung der Unsicherheit bezüglich der Ozeandiffusivitäten um einen Faktor 3 gegenüber dem Vorwissen. Dieser Lernerfolg wurde auf andere Klimacharakteristika wie Transient Climate Response (TCR) und den Temperatur Antwortparameter (α_{res}) übertragen. Wie die Schendier Experimente gezeigt haben, lassen sich ca. 0.5°C der Unsicherheit in TCR nicht durch die Klimasensitivität erklären [Held et al. (2007)]. Dies entspricht der Ausgangsstreuweite des TCR in dieser Arbeit, da andere Einflussgrößen auf die Klimasensitivität als konstant angenommen wurden und somit die Klimasensitivität in dieser Arbeit nahezu konstant bleibt. Die verbleibende Unsicherheit in TCR konnte um 0.3°C (entspricht einem Faktor von 3.8) reduziert werden. Da die TCR die Reaktion des Klimasystems auf eine Verdopplung der Kohlendioxid-Konzentration auf kurzen Zeitskalen (70 Jahre) beschreibt, konnte diese Arbeit einen alternativen Zugang zur Verbesserung von Klimaprognosen für das beginnende 21. Jahrhundert aufzeigen.

Ein weiterer Transfer des Lernerfolges bringt eine Einschränkung in der Zeitskala der Reaktion des Klimasystems auf anthropogene Treibhausgasemissionen. Diese Zeitskala beschreibt die Geschwindigkeit, mit der eine Störung der Kohlendioxidkonzentration abklingt. Der Wertebereich konnte von [20-42] auf [22-32] Jahre eingeschränkt werden. Eine kürzere Zeitkonstante bedeutet zum Einen, dass getroffene Klimaschutzmaßnahmen schneller greifen, also die Wirksamkeit möglicher Klimaschutzregime erhöht wird. Zum Anderen bedeutet dies jedoch auch, dass eine Industrie, die sich einem konkreten Temperaturziel verpflichtet hat, schneller auf alternative Technologien umrüsten muss. Wäre die Trägheit (Zeitskala) des Systems sehr hoch, so könnte man noch ein Stück länger emittieren als bisher und dann durch ambitionierten Klimaschutz umrüsten (Overshooting), bevor die Auswirkungen der Emissionen sichtbar werden. Da eine frühe Umrüstung höhere Kosten verursacht als ein späterer Umstieg, sorgt eine niedrige Zeitkonstante für höhere Kosten.

Als Ausblick dieser Arbeit wird der Einfluss des Lerneffektes bezüglich der Klimaparameter auf eine Klimaschutzpolitik beispielhaft diskutiert.

Vereinfachende Annahmen, begrenzte Verfügbarkeit von Rechenleistung und die begrenzte Auflösung und Qualität von Modell und Daten beschränken die Be-

lastbarkeit der hier erzielten Ergebnisse. Einige der konkreten Beschränkungen (die reduzierte Anzahl betrachteter Ausgabegrößen und die begrenzte Auswahl an Vergleichsdaten) werden explizit diskutiert und mögliche Erweiterungen werden gezeigt: Die Zahl betrachteter Modell-Parameter wird von zwei auf drei erhöht; entsprechend schwindet der Lerneffekt. Als erweiterte Datenbasis liefern die Salinitätsfelder eine Verbindung des Lernergebnisses bezüglich der Ozeandiffusivitäten zum Abstand der thermohalinen Zirkulation von einer Bifurkation. Diese Studie hat die Nützlichkeit Bayesschen Lernens als Werkzeug zur integrierten Behandlung eines Modell-Datenvergleichs mitsamt der Auswirkungen auf andere Ausgabegrößen bis hin zur Diskussion klimapolitischer und wirtschaftlicher Implikationen gezeigt. Da die Ergebnisse dieser Arbeit nur in der stilisierten CLIMBER-2.3 Welt gültig sind, kann diese Studie allerdings nur als Vorarbeit betrachtet werden, die zu umfangreicheren Untersuchungen mit verbesserter Datengrundlage und komplexeren Modellen animiert.

Danksagung

Mein Dank gebührt Prof. Dr. Stefan Rahmstorf und Prof. Dr. Gerald Haug für die Bereitstellung des Themas (Rahmstorf) und die Begutachtung der Arbeit. Ganz besonders möchte ich Dr. Hermann Held für seine andauernde und umfassende Betreuung sowie für die vielen wertvolle Ratschläge, Ideen und Einsichten bedanken die mir in zahlreichen fruchtbaren Diskussionen zu Teil wurden. Für die hilfreichen Hinweise und Erklärungen zum Umgang mit CLIMBER und der Natur des 8.2 ka Ereignisses danke ich Dr. Eva Bauer, Dr. Thomas Schneider von Deimling sowie Dr. Andrey Ganopolski. Für die freundliche Aufnahme, die Unterstützung in allen Fragen des Forschungsumfeldes und zeitweise finanzielle Unterstützung danke ich der ehemaligen SPARK Gruppe (jetzt Forschungsfeld III). Und schließlich danke ich ganz besonders Friederike Otto, die mir für alle Probleme dieser Arbeit als geistige Sparringspartnerin zur Seite stand.

List of Figures

2.1	Locations of the deep ice core drilling sites: GRIP (72.5°N, 37.3°W), GISP2 (72.5°N, 38.3°W), NGRIP (75.1°N, 42.3°W) and Dye3 (65.2°N, 43.8°W) (the Greenland map by S.Ekholm, Danish Cadastre / published in Nature, 431, 147-151, 2004)	8
2.2	Time series of $\delta^{18}\text{O}_{\text{ice}}$ data from four Greenland ice cores and their Kriging Mean. Time series are offset by +1.5 ‰ each against the KM.	9
2.3	(black) The Kriging Mean of the Greenland ice core data (in $\delta^{18}\text{O}_{\text{ice}}$ / offset to be displayed together with CLIMBER-2.3 output), (green) example CLIMBER-2.3 output of the cold event with added weather noise, (red) trapezoid fit to Greenland data, (blue) trapezoid fit to CLIMBER-2.3 output	10
3.1	two-dimensional parameter space of ocean diffusivities with different constraints	19
4.1	Time series of various climate variables for one realization of an 8.2 ka event simulation, showing (a) the composite freshwater forcing, (b) the NADW formation rate, (c) the temperature in Greenland [a composite of several boxes], (d) the maximum Atlantic northward heat transport, (e) global precipitation and (f) the southern hemispheric surface air temperature	25
4.2	Atlantic meridional stream function in Sv of ON (left) and INT (right) state in transient 8.2 ka event simulation. Isolines are in steps of 3 Sv.	26
4.3	Potential density of ON (left) and INT (right) state in transient 8.2 ka event simulation in kgm^{-3} above 10^3kgm^{-3} with isolines in steps of 0.4kgm^{-3}	26
4.4	Frequency of occurrence of convection events of ON (left) and INT (right) state in transient 8.2 ka event simulation with isolines in steps of 0.1.	27
4.5	Histogram of durations T of the cold event for different realizations of noise η ; parameter setting: $a_{\text{hoc}} = 2000\text{m}^2/\text{s}$, $a_v = 0.8 \cdot 10^{-4}\text{m}^2/\text{s}$, $\sigma_{\text{noise}} = 0.06 \text{ Sv}$, $D_{\text{baseline}} = 1000 \text{ yrs}$	27

List of Figures

4.6	(left) histograms for different durations of baseline flux, (right) corresponding conditional likelihood of right duration of the 8.2 ka event (160 ± 10 yrs) given the parameter setting	29
4.7	(left) Gaussian fit to the conditional likelihood $P(T \alpha = [a_{\text{hoc}}, a_v])$, (right) the same viewed from above with the half-width of the fit .	31
4.8	Transient Climate Response; dependence on the ocean diffusivities	32
4.9	Likelihood of Transient Climate Response; normalized to 1 at max; the quantiles of Ganopolski Domain (GD), Present Day Domain (SD) and the 1/e error bar (lc) of the likelihood are shown.	34
4.10	Climate sensitivity; dependence on the ocean diffusivities (over GD)	34
4.11	Temperature response parameter α_{res} over the diffusivity space covering the GD	37
4.12	Likelihood of temperature response parameter α_{res} ; normalized to 1 at max; the quantiles of Ganopolski Domain (GD), Schneider Domain (SD) and the 1/e bar (of a Gaussian fit) of the likelihood are shown	37
4.13	Likelihood of ocean response parameter μ ; normalized to 1 at max; the quantiles of Ganopolski Domain (GD), Present Day- or Schneider Domain (SD) and the 1/e error bar of the likelihood are shown	38
4.14	Likelihood of temperature response time scale $\tau = 1/\alpha_{\text{res}}$; normalized to 1 at max; the quantiles of Ganopolski Domain (GD), Present Day Domain (SD) and the 1/e error bar of the likelihood are shown	38
4.15	(left) CO_2 forcing for the TCR (blue) and a sulfate extraction (red) scenario and (right) the corresponding global mean surface temperature	39
5.1	First principal component (1st pc) of Atlantic salinity field for standard diffusivities	44
5.2	Atlantic AR(1) propagator c over the two-dimensional domain of ocean diffusivities for different values of freshwater runoff into the northern Atlantic (bottom = standard-0.1 Sv, middle = standard, upper = standard+0.1 Sv)	44
5.3	relative frequency distribution of the Atlantic AR(1) propagator c for standard value of freshwater runoff into the northern Atlantic after the Bayesian Learning on the diffusivities	45
5.4	(left) Gaussian fit to the conditional likelihood $P(T \alpha = [a_{\text{hoc}}, a_v, \text{FW} = 0.03\text{Sv}])$, (right) the same viewed from above with the half-width of the fit .	47
5.5	1/2 error bar of a Gaussian fit to the conditional likelihood $P(T \alpha = [a_{\text{hoc}}, a_v, \text{FW}])$ for different values of FW (upper: $\text{FW} = 0.015\text{Sv}$, middle: $\text{FW} = 0.03\text{Sv}$, lower: $\text{FW} = 0.045\text{Sv}$)	48

Bibliography

- Alley, R., P. Mayewski, T. Sowers, M. Stuiver, K. Taylor, and P. Clark (1997). Holocene climate instability: a prominent widespread event 8200 year ago. *Geology* 25, 483–486.
- Alley, R. B. and A. M. Ágústsdóttir (2005). The 8.2k event: cause and consequences of a major holocene abrupt climate change. *Quaternary Science Reviews* 24, 1123–1149.
- Barber, D. C., A. Dyke, C. Hillaire-Marcel, A. E. Jennings, J. T. Andrews, M. W. Kerwin, G. Bilodeau, R. McNeely, J. Southon, M. D. Morehead, and J.-M. Gagnon (1999). Forcing of the cold event of 8,200 years ago by catastrophic drainage of laurentide lakes. *Nature* 400, 344–348.
- Bauer, E., M. Claussen, V. Brovkin, and A. Hühnerbein (2003). Assessing climate forcings of the earth system for the past millenium. *Geophysical Research Letters* 30, 1276.
- Bauer, E., A. Ganopolski, and M. Montoya (2004). Simulation of the cold climate event 8200 years ago by meltwater outburst from lake agassiz. *Paleoceanography* 19, PA3014.
- Berger, A. L. (1978). Long-term variations of daily insolation and quaternary climate changes. *J. Atmos. Sci.* 35, 2362–2367.
- Bruckner, T., G. Petschel-Held, F. L. Tóth, H.-M. Füßel, C. Helm, M. Leimbach, and H.-J. Schellnhuber (1999). Climate change decision support and the tolerable windows approach. *Environmental Modeling and Assessment* 4, 217–234.
- Cavalieri, D. J., C. L. Parkinson, and K. Y. Vinnikow (2003). 30-year satellite record reveals contrasting arctic and antarctic sea ice variability. *Geophys Res Lett* 30, 173–200.
- Clark, P. U. (2001). Freshwater forcing of abrupt climate change during the last glaciation. *Science* 293, 283–287.
- Crowley, T. J. (1992). North atlantic deep water cools the southern hemisphere. *Paleoceanography* 7, 489–497.

Bibliography

- Cuffey, K. M. and G. D. Clow (1997). Temperature, accumulation, and ice sheet elevation in central greenland through the last deglacial transition. *J. Geophys. Res.* 102, 26,383–26,389.
- Dahl-Jensen, D., K. Mosegaard, N. Gundestrup, G. D. Clow, S. J. Johnsen, A. W. Hansen, and N. Balling (1998). Past temperatures directly from the greenland ice sheet. *Science* 282, 268–271.
- Dansgaard, W. (1985). Greenland ice core studies. *Paleogeography, Paleoclimatology and Paleoecology* 50, 185–187.
- Dansgaard, W. (1993). Evidence for general instability of past climate from a 250 kyr ice record. *Nature* 364, 218–220.
- Ganachaud, A. and C. Wunsch (2003). Large-scale ocean heat and freshwater transports during the world ocean circulation experiment. *J Clim* 16, 696–705.
- Ganopolski, A., V. K. Petoukhov, S. Rahmstorf, V. Brovkin, M. Claussen, A. Eliseev, and C. Kubatzki (2001). Climber-2: A climate system model of intermediate complexity. part ii: Sensitivity experiments. *Climate Dynamics* 17, 735–751.
- Ganopolski, A. and S. Rahmstorf (2001). Rapid changes of glacial climate simulated in a coupled climate model. *Nature* 409, 153–158.
- Ganopolski, A., S. Rahmstorf, V. Petoukhov, and M. Claussen (1998). Simulation of modern and glacial climate with a coupled model of intermediate complexity. *Nature* 391, 351–356.
- GRIP-Project-Members (1993). Climate instability during the last interglacial period recorded in the grip ice core. *Nature* 364, 203–207.
- Held, H. (2007). Bayesian learning for stochastic climber-2. *unpublished*.
- Held, H. and T. Kleinen (2004). Detection of climate system bifurcations by degenerate fingerprinting. *Geophysical Research Letters* 31, L23207.
- Held, H., E. Kriegler, K. Lessmann, and O. Edenhofer (2007). Cost effective climate policies optimized under technology and climate uncertainty. *under revision for Energy Economics*.
- Howson, C. and P. Urbach (1991). Bayesian reasoning in science. *Nature* 350, 371–374.
- Johnsen, S. J., H. B. Clausen, W. Dansgaard, K. Fuhrer, N. Gundestrup, C. U. Hammer, P. Iversen, J. Jouzel, B. Stauffer, and J. P. Steffensen (1992). Irregular glacial interstadials recorded in a new greenland ice core. *Nature* 359, 311–313.

- Johnsen, S. J., D. Dahl-Jensen, W. Dansgaard, and N. Gundestrup (1995). Greenland paleo temperatures derived from grip borehole temperature and ice core isotope profiles. *Tellus, Ser. B* 47, 624–629.
- Johnsen, S. J., D. Dahl-Jensen, W. Dansgaard, N. Gundestrup, J. P. Steffensen, H. B. Clausen, H. Miller, V. Masson-Delmotte, E. Sveinbjørnstadttir, and J. White (2001). Oxygen isotope and paleo temperature records from six greenland icecore stations: Camp century, dye-3, grip, gisp2, renland and northgrip. *J. Quat. Sci.* 16, 299–307.
- Jones, P. D., M. New, D. E. Parker, S. Martin, and I. G. Rigor (1999). Surface air temperature and its changes over the past 150 years. *Rev Geophys* 37, 173–200.
- Kleinen, T., H. Held, and G. Petschel-Held (2003). The potential role of spectral properties in detecting thresholds in the earth system: application to the thermohaline circulation. *Ocean Dynamics* 53, 53–63.
- Klitgaard-Kristensen, D., H. P. Sejrup, H. Hafidason, S. Johnsen, and M. Spurk (1998). A regional 8200 cal. yr bp cooling event in northwest europe, induced by final stages of the laurentide ice-sheet deglaciation? *Journal of Quaternary Sciences* 13, 165–169.
- Kriegler, E. and T. Bruckner (2005). Sensitivity analysis of emissions corridors for the 21st century. *Climatic Change* 66, 345–387.
- Legates, D. R. (1995). Global and terrestrial precipitation- a comparative-assessment of existing climatologies. *Int J Climatol* 15, 237–258.
- Leuenberger, M. C., C. Lang, and J. Schwander (1999). Delta ($\delta^{15}\text{N}$) measurements as a calibration tool for the paleothermometer and gas-ice age differences: a case study for the 8200 bp event on grip ice. *Journal of Geophysical Research* 104, 22163–22170.
- Leverington, D. W., J. D. Mann, and J. Teller (2002). Changes in the bathymetry and volume of glacial lake agassiz between 9200 and 7700 ^{14}C yr bp. *Quaternary Research* 57, 244–252.
- Liccardi, J. M., J. T. Teller, and P. U. Clark (1999). Freshwater routing by the laurentide ice sheet during the last deglaciation. in: U. p. clark, r. s. webb, l. d. keigwin (eds.), mechanisms of global climate change at millennial time scales. *American Geophysical Union, Washington DC Geophysical Monograph* 112, 177–201.
- Marshall, S. J. and G. K. C. Clarke (1999). Modelling north american freshwater runoff through the last glacial cycle. *Quat. Res.* 52, 300–315.

Bibliography

- Mayewski, P. A., L. D. Meeker, S. Whitlow, M. S. Twickler, M. C. Morisson, P. Bloomfield, G. C. Bond, R. B. Alley, A. J. Gow, P. M. Grootes, D. A. Meese, M. Ram, K. C. Taylor, and W. Wumkes (1994). Changes in atmospheric circulation and ocean ice cover over the north atlantic during the last 41,000 years. *Science* *263*, 1747–1751.
- Muscheler, R., J. Beer, and M. Vonmoos (2004). Causes and timing of the 8200 year bp event inferred from the comparison of the grip be-10 and the tree ring delta c-14 record. *Quaternary Science Reviews* *23*, 2101–2111.
- NGRIP-Project-Members (2004). High-resolution record of northern hemisphere climate extending into the last interglacial period. *Nature* *432*, 147–151.
- Petoukhov, V., A. Ganopolski, V. Brovkin, M. Claussen, A. Eliseev, C. Kubatzki, and S. Rahmstorf (2000). Climber-2: a climate system model of intermediate complexity. part i: model description and performance for present climate. *Climate Dynamics* *16*, 1–17.
- Petschel-Held, G., H.-J. Schellnhuber, T. Bruckner, F. L. Tóth, and K. Hasselmann (1999). The tolerable windows approach: Theoretical and methodological foundations. *Climatic Change* *41*, 303–331.
- Rahmstorf, S. (2002). Ocean circulation and climate during the past 12,000 years. *Nature* *419*, 207–214.
- Rasmussen, S., K. Andersen, A. Svensson, J. Steffensen, B. Vinther, H. Clausen, M.-L. Siggaard-Andersen, S. Johnsen, L. Larsen, M. Bigler, R. Röthlisberger, H. Fischer, K. Goto-Azuma, M. Hansson, and U. Ruth (2006a). A new greenland ice core chronology for the last glacial termination. *Journal of Geophysical Research* *111*, D06102.
- Rasmussen, S. O., K. K. Andersen, A. M. Svensson, J. P. Steffensen, B. M. Vinther, H. B. Clausen, M.-L. Siggaard-Andersen, S. J. Johnsen, L. B. Larsen, M. Bigler, R. Röthlisberger, H. Fischer, K. Goto-Azuma, M. E. Hansson, and U. Ruth (2006b). A new greenland ice core chronology for the last glacial termination. *Journal of Geophysical Research* *111*, D06102.
- Renssen, H., H. Goose, and T. Fichefet (2002). Modeling the effect of freshwater pulses on early holocene climate: The influence of high-frequency climate variability. *Paleoceanography* *17*, 1020.
- Renssen, H., H. Goose, T. Fichefet, and J. Campin (2001). The 8.2 kyr bp event simulated by a global atmosphere-sea-ice-ocean model. *Geophys. Res. Lett.* *28*, 1567–1570.

- Renssen, H., H. Goose, and R. Muscheler (2006). Coupled climate model simulation of holocene cooling events: oceanic feedback amplifies solar forcing. *Clim. Past* 2, 79–90.
- Rohling, E. J. and H. Pälike (2005). Centennial-scale climate cooling with a sudden cold event around 8,200 years ago. *Nature* 434, 975–979.
- Schmittner, A. and A. J. Weaver (2001). Dependence of multiple climate states on ocean mixing parameters. *Geophysical Research Letters* 28, 1027–1030.
- Talley, L. D., J. L. Reid, and P. E. Robbins (2003). Data-based meridional overturning stream functions for the global ocean. *J Clim* 16, 3213–3226.
- Teller, J. T., D. W. Leverington, and J. D. Mann (2002). Freshwater outbursts to the oceans from glacial lake agassiz and their role on climate change during the last deglaciation. *Quaternary Science Reviews* 21, 879–887.
- Thomas, E. R., E. W. Wolff, R. Mulvaney, J. P. Steffensen, S. J. Johnsen, C. Arron-Smith, J. W. White, B. Vaughn, and T. Popp (2007). The 8.2k event from greenland ice cores. *Quaternary Science Reviews* 26, 70–81.
- Tóth, F. L., T. Bruckner, H.-M. Füßel, M. Leimbach, G. Petschel-Held, and H.-J. Schellnhuber (1997). The tolerable window approach to integrated assessments. In *Climate Change and Integrated Assessment Models - Bridging the gaps. Proceedings of the IPCC Asia-Pacific Workshop on Integrated Assessments Models*, pp. 403–440. Center for Global Environmental Research.
- von Deimling, T. S., H. Held, A. Ganopolski, and S. Rahmstorf (2006). Climate sensitivity estimated from ensemble simulations of glacial climate. *Climate Dynamics* 27, 149–163.
- von Grafenstein, U., H. Erlenkeuser, A. Brauer, J. Jouzel, and S. Johnsen (1999). A mid-european decadal isotope-climate record from 15,000 to 5000 years b. p. *Science* 284, 1654–1657.
- Wackernagel, H. (1995). *Multivariate Geostatistics* (1st ed.). Springer-Verlag Berlin Heidelberg New York.
- Walsh, J. E. and D. H. Portis (1999). Variations of precipitation and evaporation over the north atlantic ocean, 1958-1997. *Journal of Geophysical Research* 104, 16,613–16,631.
- Wiersma, A. P. and H. Renssen (2006). Model-data comparison for the 8.2ka bp event: confirmation of a forcing mechanism by catastrophic drainage of laurentide lakes. *Quaternary Science Reviews* 25, 63–88.

Bibliography

Wright, D. G. and T. F. Stocker (1991). A zonally averaged ocean model for the thermohaline circulation. part i: Model development and flow dynamics. *J. Phys. Oceanogr.* *21*, 1713–1724.

List of abbreviations

AR(1)	one-dimensional autoregressive process
BP	before present (1950)
CLIMBER	CLIMate-BiospERe model
EMIC	Earth system model of intermediate complexity
EOF	empirical orthogonal function
GCM	Global Circulation Model
GWP	Global Welfare Product
iid	identically independent distributed
IPCC	Intergovernmental Panel on Climate Change
LIS	Laurentic Ice Sheet
NADW	North Atlantic Deep Water
NH	northern hemisphere
ppm	parts per million
SST	sea surface temperature
THC	Thermohaline Circulation
yrs	years

Hiermit versichere ich, die vorliegende Diplomarbeit ohne Hilfe Dritter nur mit den angegebenen Quellen und Hilfsmitteln angefertigt zu haben. Alle Stellen, die aus Quellen entnommen wurden, sind als solche kenntlich gemacht worden. Diese Arbeit hat in gleicher oder ähnlicher Form noch keiner Prüfungsbehörde vorgelegen.

Potsdam, den 18. Oktober 2007

Alexander Lorenz